

1 **Host influenced geochemical signature in the parasitic foraminifer *Hyrrokkin sarcophaga***

2 Nicolai Schleinkofer^{1,2}, David Evans^{1,2}, Max Wisshak³; Janina Vanessa Büscher^{4,5}, Jens Fiebig^{1,2}, André Freiwald³, Sven Härter¹,
3 Horst R. Marschall^{1,2}, Silke Voigt^{1,2}, Jacek Raddatz^{1,2}

4 ¹Goethe Universität Frankfurt, Institut für Geowissenschaften, Frankfurt am Main, Germany

5 ²Goethe Universität Frankfurt, Frankfurt Isotope and Element Research Center (FIERCE), Frankfurt am Main, Germany

6 ³Senckenberg am Meer, Marine Research Department, Wilhelmshaven, Germany

7 ⁴National University of Ireland Galway, Department of Earth and Ocean Sciences, Galway, Ireland

8 ⁵GEOMAR Helmholtz Centre for Ocean Research Kiel, Department of Biological Oceanography, Kiel, Germany

9 Corresponding Author: Nicolai Schleinkofer (schleinkofer@em.uni-frankfurt.de)

10 **Abstract**

11 *Hyrrokkin sarcophaga* is a parasitic foraminifera that is commonly found in cold-water coral reefs
12 where it infests the file clam *Acesta excavata* and the scleractinian coral *Desmophyllum pertusum*
13 (formerly known as *Lophelia pertusa*). Here, we present measurements of the trace-element and
14 isotopic composition of these parasitic foraminifera, analyzed by inductively coupled optical emission
15 spectrometry (ICP-OES), electron probe micro analysis (EPMA) and mass spectrometry (Gas-source-
16 MS and Inductively-coupled-plasma-MS).

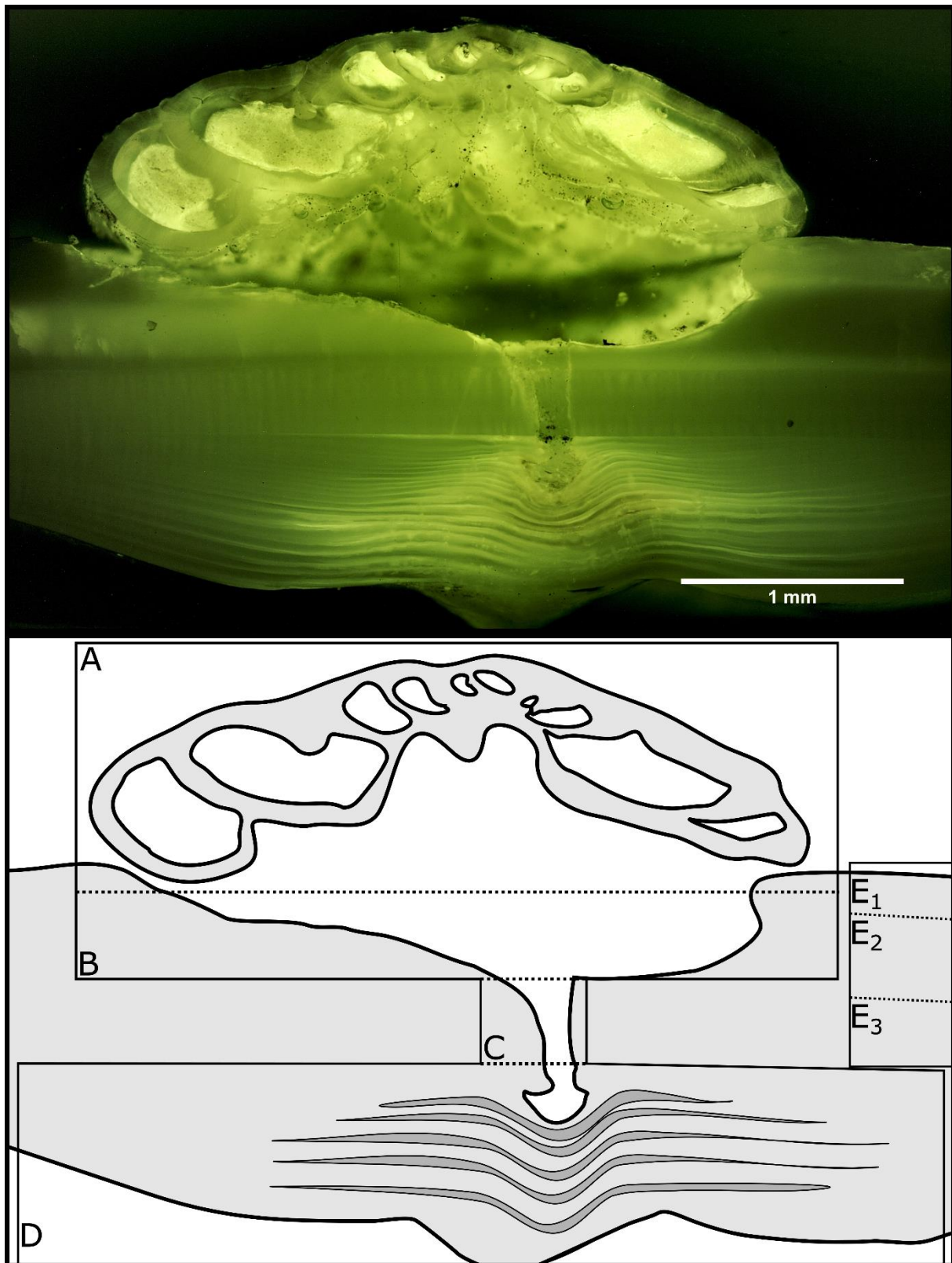
17 Our results reveal that the geochemical signature of *H. sarcophaga* depends on the host organism it
18 infests. Sr/Ca ratios are 1.1 mmol mol⁻¹ higher in *H. sarcophaga* that infest *D. pertusum*, which could
19 be an indication that dissolved host carbonate material is utilised in shell calcification, given that the
20 aragonite of *D. pertusum* has a naturally higher Sr concentration compared to the calcite of *A.*
21 *excavata*. Similarly, we measure 3.1 ‰ lower δ¹³C and 0.25 ‰ lower δ¹⁸O values in *H. sarcophaga* that
22 lived on *D. pertusum*, which might be caused by the direct uptake of the host's carbonate material with
23 a more negative isotopic composition or different pH regimes in these foraminifera (pH can exert a
24 control on the extent of CO₂ hydration/hydroxylation) due to the uptake of body fluids of the host. We
25 also observe higher Mn/Ca ratios in foraminifera that lived on *A. excavata* but did not penetrate the
26 host shell compared to specimen that penetrated the shell, which could be interpreted as a change in
27 food source, changes in the calcification rate, Rayleigh fractionation or changing oxygen conditions.

28 While our measurements provide an interesting insight into the calcification process of this unusual
29 foraminifera, these data also indicate that the geochemistry of this parasitic foraminifera is unlikely to
30 be a reliable indicator of paleoenvironmental conditions using Sr/Ca, Mn/Ca, δ¹⁸O or δ¹³C unless the
31 host organism is known and its geochemical composition can be accounted for.

32

33 **1. Introduction**

34 The foraminifera are a very diverse group of marine shelly organisms that are commonly used for
35 paleoenvironmental reconstructions using the isotopic or elemental composition of their carbonate
36 shell (Petersen et al., 2018; Hönisch et al., 2011; Gray and Evans, 2019; Lear and Rosenthal, 2006;
37 Raddatz et al., 2017). They first appeared in the Cambrian (Culver, 1991) and, over the course of the
38 Phanerozoic, occupied oceanic settings from coastal waters to the open ocean, as well as deep sea
39 benthic habitats (Goldstein, 1999). Multiple feeding methods are known from foraminifera, including
40 suspension feeding, grazing, predation and parasitic feeding (Hancock et al., 2015). The latter is
41 probably the least common feeding mechanism among the foraminifera with only nine species that
42 are known to be parasitic and a further 13 that are suspected to be (Walker et al., 2017). One of the
43 known parasitic species is *Hyrrokin sarcophaga* (Cedhagen, 1994), a common foraminifera in cold-
44 water coral reefs in the NE-Atlantic (Beuck et al., 2008). *H. sarcophaga* preferentially colonises the file
45 clam *Acesta excavata*, but also other organisms such as the bivalve *Delectopecten vitreus*, sponges of
46 the family Geodiidae and Ancorinidae, cold-water corals such as *Desmophyllum pertusum* (formerly
47 known as *Lophelia pertusa* (Addamo et al., 2016)), *Madrepora oculata* and *Flabellum japonicum*, as
48 well as other foraminifera (Beuck et al., 2008; Cheng and Dai, 2016; Cedhagen, 1994). Besides biogenic
49 hard substrates, *H. sarcophaga* can also be found settling on rocks which shows that it can at least
50 survive short periods without a host (Cedhagen, 1994). *H. sarcophaga* forms an attachment etching,
51 i.e. mirroring its spiral outline on the host. From this depression the foraminifera etch a canal into the
52 shell of the host (Cedhagen, 1994) (Fig. 1). This allows the foraminifera to feed on the bivalve host's
53 tissue (Cedhagen, 1994) and possibly assimilate amino acids from its extrapallial calcifying fluid
54 (Schweizer et al., 2012; Alexander and Delaca, 1987).



55

56 Figure 1 Fluorescence microscopic image (excitation 420 – 490 nm) and schematic figure of *H. sarcophaga* on *A. excavata*. A:
 57 *H. sarcophaga*, B: Attachment depression corroded by *H. sarcophaga*, C: Bored canal, D: Callus built by *A. excavata* (SRZ =
 58 shell repair zone), E: Undisturbed shell, E₁: Calcitic shell layer (fibrous), E₂: Calcitic shell layer (microgranular), E₃: Aragonitic
 59 shell layer

60

61 The bivalve reacts by building a callus (layered aragonite rich in organics) to seal this boring (Fig 1D)
62 and defend the organism from the parasite's attack (Beuck et al., 2008). In *D. pertusum*, borings into
63 the inner calyx area were not observed (Beuck et al., 2008). Instead, multiple "whip"-shaped tunnels
64 protrude into the coral's skeleton, which possibly serve an anchoring function (Beuck et al., 2008). The
65 pit is possibly formed either as a way to protect itself from cleaning attempts of the host and increase
66 attachment strength or to serve the foraminifera's need for calcium and/or DIC (Beuck et al., 2008;
67 Cedhagen, 1994).

68 As the parasitic foraminifera ingests material from its host, the question arises whether this process
69 exerts an influence on the shell geochemistry of the parasite. Should this be the case, this factor may
70 need to be accounted for, especially as some parasitic foraminifera, such as *Cibicides refulgens*, are
71 also used in geochemical studies for paleoenvironmental reconstructions (García-Gallardo et al., 2017;
72 Mackensen and Nam, 2014; Rathburn and de Deckker, 1997; Raddatz et al., 2011; Alexander and
73 Delaca, 1987).

74 Here, we present element to Ca ratios (Mg/Ca, Sr/Ca, Na/Ca and Mn/Ca) and stable isotope data
75 (oxygen and carbon) analyzed in *H. sarcophaga* collected from different host organisms (*A. excavata*
76 and *D. pertusum*) from the Trondheimsfjord (Norway) to explore if and how the different hosts
77 influence the geochemical composition of the test of foraminifera. In addition, we present element
78 maps analyzed by electron microprobe analysis (EPMA) of the callus region of *A. excavata* in order to
79 explore geochemical differences between the callus region and undisturbed shell areas.

80 **2. Material and Methods**

81 **2.1. Sampling**

82 All investigated samples were collected in the Leksa Reef, located at the entrance to the
83 Trondheimsfjord in Norway (N 63.613056/E 9.384167, depth ~ 200 m) by means of the manned
84 submersible JAGO (GEOMAR Helmholtz-Zentrum für Ozeanforschung, 2017) during the scientific
85 cruises POS473 and POS525 with RV *Poseidon* (Form et al., 2015; Büscher, 2018; GEOMAR Helmholtz-
86 Zentrum für Ozeanforschung, 2015). In total we analyzed 30 specimens of *H. sarcophaga*, which were
87 divided into three groups: 1. *H. sarcophaga* that infested *A. excavata* with callus formation (henceforth
88 called HAW), 2. *H. sarcophaga* that infested *A. excavata* without callus formation (henceforth called
89 HAO; HAW + HAO = HA), 3. *H. sarcophaga* that infested *D. pertusum* (henceforth called HL). Samples
90 of *A. excavata* and *D. pertusum* were alive when sampled. We cannot be entirely certain that *H.*
91 *sarcophaga* were still alive when sampled, but upon death they easily become detached from the shell
92 whereas in our samples the foraminifera were still firmly attached. For ICP-OES, ICP-MS and GS-MS,

93 the samples were ultrasonically rinsed in deionized water for five minutes and allowed to dry before
94 crushing in an agate mortar

95 **2.2. Shell carbonate polymorph**

96 The polymorph of the foraminiferal shell was determined using cobalt nitrate solution (Meigen
97 solution). The foraminifera samples were crushed in an agate mortar and transferred to Eppendorf
98 containers. The samples were mixed with 10 wt% $\text{Co}(\text{NO}_3)_2$ aqueous solution and allowed to react at
99 95°C for 20 minutes. Afterwards the samples were washed four times with deionized-water and
100 inspected under a KEYENCE VHX-S660E microscope. Aragonite stains purple/pink in cobalt nitrate
101 solution, whereas calcite remains unaffected (Kato et al., 2003)

102 **2.3. Fluorescence microscopy**

103 We used fluorescence microscopy to investigate the distribution of the organic material in the
104 foraminifera and the underlying bivalve shell. The sample was cut, ultrasonically cleaned in deionized-
105 water, embedded in epoxy resin (Araldite 2020) and polished with $3\ \mu\text{m}$ diamond-lapping paste
106 Fluorescent images were taken using a Leica DMRX-POL microscope with fluorescent front light and a
107 50 W mercury lamp. The microscope was equipped with an H3 filter cube, which excites in the
108 wavelength range of blue to violet (Bandpass filter: 420 – 490 nm) The pictures were taken with a
109 digital camera connected to the microscope with 0.25 s exposure time.

110 **2.4. EPMA**

111 Two samples of *A. excavata* with attached *H. sarcophaga* were analysed by electron probe micro
112 analysis (EPMA). The area of interest was cut from the shell with a handheld drilling tool, ultrasonically
113 cleaned in deionized-water for five minutes, mounted vertically into circular mounts and embedded in
114 epoxy resin (Araldite 2020). The sample surface was ground with $9\ \mu\text{m}$ grid with silicon carbide sanding
115 paper and then polished using $3\ \mu\text{m}$ diamond-water based lapping paste. After polishing the samples
116 were coated with carbon.

117 The EPMA analyses were conducted at Goethe University Frankfurt on a JEOL JXA-8530F Plus Field
118 Emission Gun Electron Probe Micro Analyzer (FEG-EPMA). Analysis conditions were: 15 kV acceleration
119 voltage, 20 nA current with a beam diameter of $3\ \mu\text{m}$. We used a TAP crystal for Mg, TAPL for Na and
120 Sr and PETH for S. Detection limits are calculated with the equation given in Goldstein et al., 2017 and
121 amount to: $\text{Mg} = 178\ \mu\text{g g}^{-1}$ ($\text{Mg}/\text{Ca} = 0.7\ \text{mmol mol}^{-1}$), $\text{Na} = 170\ \mu\text{g g}^{-1}$ ($\text{Na}/\text{Ca} = 0.7\ \text{mmol mol}^{-1}$), $\text{Sr} =$
122 $129\ \mu\text{g g}^{-1}$ ($\text{Sr}/\text{Ca} = 0.1\ \text{mmol mol}^{-1}$), $\text{S} = 152\ \mu\text{g g}^{-1}$ ($\text{S}/\text{Ca} = 0.4\ \text{mmol mol}^{-1}$) and $\text{Ca} = 195\ \mu\text{g g}^{-1}$. Molar
123 ratios were calculated from the weight fractions of the specific oxides (CaO , MgO , Na_2O , SrO , SO_3) by
124 calculating the concentration of the observed elements (in $\mu\text{g/g}$) and normalization to Ca accounting

125 for their relative atomic mass. The chemical maps were recorded with a beam diameter of 2 μm , 15
126 kV acceleration voltage and 20 nA current.

127 **2.5. ICP-OES**

128 For ICP-OES measurements we used ten HAW, ten HAO and ten HL samples. About 120 μg of sample
129 powder was transferred to Eppendorf tubes (acid cleaned with 5 % HNO_3) and sealed. Each sample
130 was analyzed three times.

131 Elemental ratios Mg/Ca, Sr/Ca, Na/Ca and Mn/Ca (only for foraminifera and bivalves) were analyzed
132 by inductively coupled plasma-optical emission spectrometry (ICP-OES). ICP-OES analysis was carried
133 out using a ThermoScientific iCap 6300 Duo at the Institute of Geosciences, Goethe University
134 Frankfurt. The sample powder ($\approx 140 \mu\text{g}$) was dissolved in 500 μL HNO_3 (2%) and 300 μL aliquots were
135 separated. Subsequently 1500 μL of 1.2 mg L^{-1} yttrium solution was added to each aliquot as an internal
136 standard resulting in a concentration of Y = 1 mg L^{-1} and Ca = 25 mg L^{-1} . The intensity data were
137 background corrected, standardized internally to Y and normalized to Ca. Accuracy is reported in %-
138 deviation from values of standard reference material JCP1 and USGS MACS-3 (n = 5)(Jochum et al.,
139 2005) and is better than 1% for Mg/Ca and Sr/Ca, 5% for Na/Ca and 3% for Mn/Ca. Precision is reported
140 in relative standard deviation; % RSD of the USGS MACS-3 and JCP1 carbonate reference material (n =
141 5)(Jochum et al., 2005) and is better than 3% for all analyzed elements.

142 Bivalve (n = 3) and coral (n = 3) samples were treated similarly to foraminifera samples. We took 15 -
143 20 samples per shell from the outermost shell section along the main growth axis, starting at the
144 ventral margin resulting in a total of 49 samples. The corals were sampled randomly over the whole
145 calyx area resulting in 44 samples.

146 **2.6. ICP-MS**

147 The manganese concentration of *D. pertusum* had to be determined by ICP-MS because it was below
148 the limit of detection by ICP-OES. We used three specimens (two from the Leksa Reef, one from the
149 Sula Reef) of which we sampled 150 μg from the fibrous shell section. Each sample was measured
150 twice.

151 For solution based ICP-MS measurements we used 150 μg of sample powder and dissolved it in 500 μL
152 2% HNO_3 . The dissolved sample (300 μL) was mixed with 1500 μL 1.2 mg L^{-1} yttrium solution which was
153 used as the internal standard. The reference material ECRM 752-1 (Greaves et al., 2008) was used to
154 monitor measurement precision and accuracy, reported in %-deviation from the reported values of
155 the standard reference material ECRM 752-1 (n = 3) (Greaves et al., 2005) and equals 7% for this

156 analytical session. Precision is reported in relative standard deviation; % RSD of the ECRM 752
157 carbonate reference material (n= 3) is better than 1% for Mn/Ca

158 **2.7. Stable oxygen and carbon isotopes**

159 We used nine HAW, nine HAO and ten HL for stable isotope measurements. About 100 µg of sample
160 powder was transferred to borosilicate glass tubes and sealed with plastic caps. Each sample was
161 measured three times.

162 Stable isotopes were measured at Goethe University Frankfurt on a Thermo MAT 253 Mass
163 Spectrometer interfaced with a Thermo Fisher Scientific GasBench II. The sample material (100 µg) was
164 reacted with 99% H₃PO₄ at 72°C in continuous flow mode. Analytical procedures followed Spótl and
165 Vennemann (2003). δ¹³C and δ¹⁸O values are reported in δ-notation, i.e. ‰-deviation relative to Vienna
166 Pee Dee Belemnite (VPDB) and Vienna Standard Mean Ocean (VSMOW), respectively. Internal
167 precision is better than 0.06‰ (δ¹³C) and 0.08‰ (δ¹⁸O).

168 Samples of the ambient water were collected during scientific cruise POS525 with R/V *Poseidon* in July
169 2018 (Büscher, 2018; GEOMAR Helmholtz-Zentrum für Ozeanforschung, 2015). A Rosette Sampler
170 equipped with conductivity, temperature and depth sensors (CTD, Sea-Bird Scientific. SBE 911 Plus)
171 was used to sample water from the investigated reefs. The water samples were transferred from 12 L
172 Niskin bottles to 250 mL borosilicate bottles and sealed after adding 100 µL HgCl₂ to prevent biological
173 activity of microorganisms that may alter the isotopic composition. The samples were stored in a fridge
174 at 4°C until measurement.

175 Water samples were analyzed for their isotopic composition at Friedrich-Alexander University
176 Erlangen-Nürnberg by an automated equilibration unit (Gasbench II; Thermo Fisher Scientific) coupled
177 in continuous flow mode to a Delta *plus* XP isotope ratio mass spectrometer (Thermo Fisher Scientific,
178 Bremen, Germany).

179 Water for δ¹³C analyses was extracted from the sample bottles by a 1-mL disposable syringe through
180 the septa without opening the bottle to avoid loss of CO₂ during sample transfer. During water
181 extraction, the removed volume was simultaneously replaced by inert gas through a second needle
182 connected to an argon-filled gas sampling bag (Grace, Deerfield, IL, USA). The samples were injected
183 into 12 mL Labco Exetainers™ (Labco Ltd. Lampeter, U.K) that were prepared with phosphoric acid and
184 pre-flushed with helium (purity 99.999%). For seawater the injection volume was 0.85 mL per vial.
185 Samples were analyzed in duplicates and the reported values are arithmetic means. All values are
186 reported in the standard δ-notation in per mille (‰) vs. VPDB.

187 Sample bottles for $\delta^{18}\text{O}$ were de-capped and 0.5 mL water were extracted with a pipette for CO_2
188 equilibration. The samples were transferred into 12 mL Labco Exetainers™ (Labco Ltd. Lampeter, U.K)
189 and subsequently flushed with 0.3% CO_2 in helium. Equilibration time was 24 hours at 25 °C. All samples
190 were measured in duplicates and the reported values are arithmetic means. All values are reported in
191 the standard δ -notation in per mille (‰) vs. VSMOW. External reproducibility based on repeated
192 analysis of control samples was better than 0.1‰ and 0.05‰ for $\delta^{13}\text{C}$ and $\delta^{18}\text{O}$, respectively.

193 **2.8. Statistical computation**

194 We used one-way ANOVA to test the effect of the host species on the elemental and isotopic
195 composition in *H. sarcophaga*. Shapiro-Wilk test and Levene's test were used to ensure normal
196 distribution and equal variance of the target variables. Most groups and target variables are normally
197 distributed except for Na/Ca in the HAO group and $\delta^{18}\text{O}$ in the HL group. All target variables except for
198 Mn/Ca and Sr/Ca show equal variance based on the Levene's test. Normal distribution and equal
199 variance are considered a prerequisite for ANOVA. As these prerequisites are not met in some sample
200 groups, we additionally tested the data with a Kruskal-Wallis test which is a non-parametric alternative
201 to ANOVA (Lantz, 2013). Pairwise comparison of the different groups was accomplished with
202 Bonferroni adjusted Tuckey-HSD test. To test the relationship between different variables we used a
203 linear regression model fitted with ordinary least squares (OLS). All reported p -values are Bonferroni
204 adjusted. Some measurements could be considered outliers, based on the interquartile range (IQR);
205 $Q1 - 1.5 \cdot \text{IQR}$ and $Q3 + 1.5 \cdot \text{IQR}$. However, we have not truncated these measurements because most
206 of them are just slightly outside the range mentioned above. Only one measurement shows a high
207 deviation, but keeping it in the dataset does not change the outcome of the analysis.

208 **3. Results**

209 **3.1. Carbonate Polymorph**

210 The investigated *H. sarcophaga* samples show no staining (Supplement S1) under the influence of
211 cobalt nitrate solution. Consequently, the shells are calcitic as is the case for other species of the order
212 Rotaliida (Horton et al., 2021).

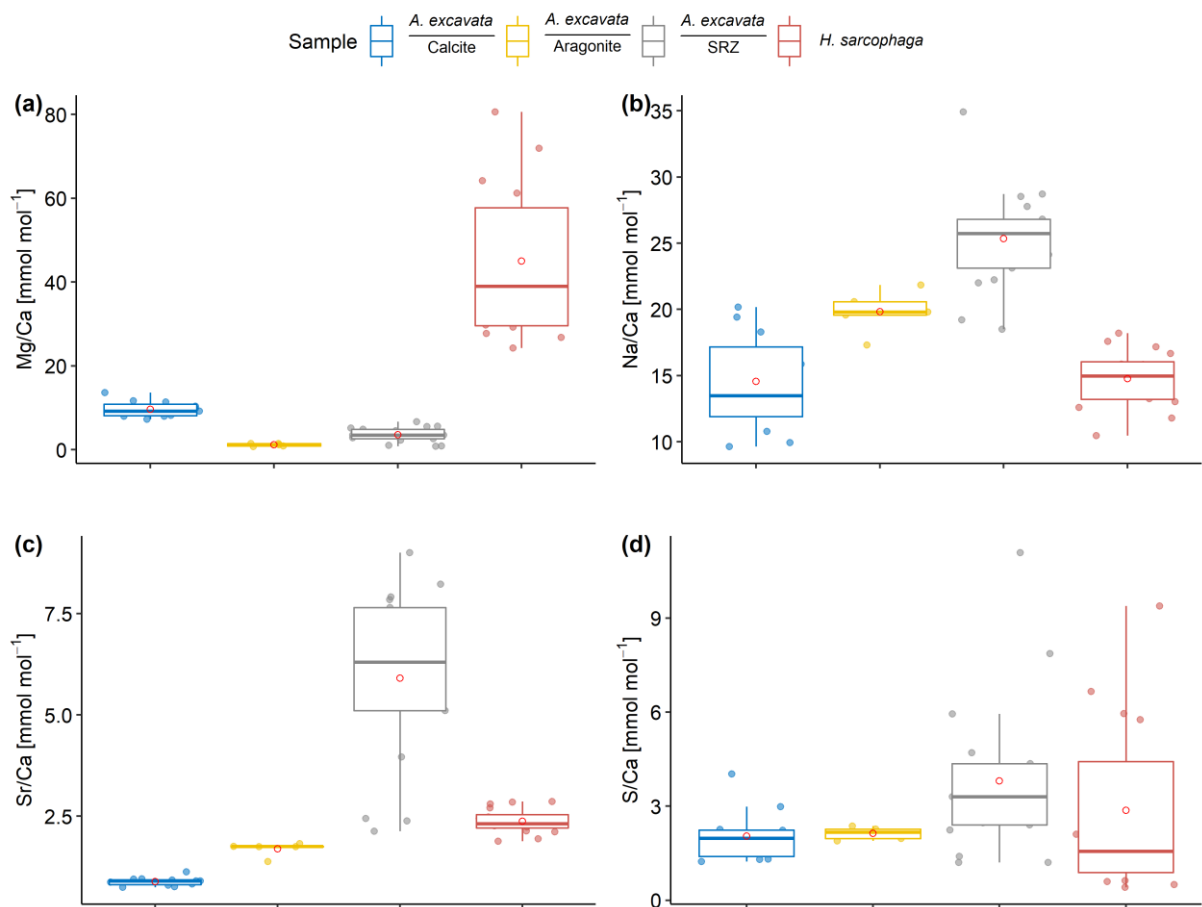
213 **3.2. Fluorescence microscopy**

214 The fluorescence microscopic image of *H. sarcophaga* attached to *A. excavata* (Fig. 1) shows distinct
215 fluorescent and non-fluorescent layers in the shell repair zone (SRZ) of the bivalve. Highly fluorescent
216 material is also observable on *H. sarcophaga*, especially in the test apertures.

217 The SRZ has a maximum thickness of 900 μm , decreasing in all directions. The fluorescent layers in the
218 SRZ are 20 – 40 μm thick. These layers taper off distally from the bore canal and disappear. Non-

219 fluorescent layers are generally smaller ranging from 9- 20 μm . The asymmetric pit that is produced by
 220 the foraminifera is observable, one side of the pit is rising steeply whereas the other side has a
 221 shallower angle. The bore canal, which starts at the bottom of the attachment etching, is 400 μm long
 222 in the undisturbed bivalve shell, but continues in the callus by another 240 μm . At the start of the bore
 223 the canal is 340 μm in diameter and continuously narrows to 140 μm . The canal ends in the SRZ with
 224 a “mushroom-like” shape.

225 **3.3. Element composition of point measurements (EPMA)**



226

227 Figure 2 Results of point measurements by EPMA in different sections of *A. excavata* and *H. sarcophaga* (two specimens
 228 each). A: Mg/Ca, B: Na/Ca, C: Sr/Ca, D: S/Ca. Boxes display the interquartile range (IQR) and lines the median values. The
 229 whiskers show min and max values that are within the range of $Q1 - 1.5 * IQR - Q3 + 1.5 * IQR$. Red circles show the mean values.
 230 Sample size = 11, 5, 17, 16 (Calcite, Aragonite, SRZ, *H. Sarcophaga*). Text below the horizontal lines in the legend is the sampled
 231 area.

232 Table 1 Wilcoxon-Mann-Whitney test results of E/Ca comparison between the observed shell sections. Bold fields show
 233 significant differences between the two groups. *p*-values are Bonferroni adjusted.

Wilcoxon-Mann-Whitney Test			
	Group 1	Group 2	<i>p</i>
Mg/Ca	Calcite	Aragonite	0.003
	Calcite	SRZ	<0.001
	Calcite	<i>H. sarcophaga</i>	<0.001

	Aragonite	SRZ	0.051
	Aragonite	<i>H. sarcophaga</i>	<0.001
	SRZ	<i>H. sarcophaga</i>	<0.001
Na/Ca	Calcite	Aragonite	0.052
	Calcite	SRZ	<0.001
	Calcite	<i>H. sarcophaga</i>	1
	Aragonite	SRZ	0.027
	Aragonite	<i>H. sarcophaga</i>	0.002
	SRZ	<i>H. sarcophaga</i>	<0.001
	Calcite	Aragonite	0.003
Sr/Ca	Calcite	SRZ	<0.001
	Calcite	<i>H. sarcophaga</i>	<0.001
	Aragonite	SRZ	<0.001
	Aragonite	<i>H. sarcophaga</i>	<0.001
	SRZ	<i>H. sarcophaga</i>	<0.001
	Calcite	Aragonite	1
S/Ca	Calcite	SRZ	0.116
	Calcite	<i>H. sarcophaga</i>	1
	Aragonite	SRZ	0.286
	Aragonite	<i>H. sarcophaga</i>	1
	SRZ	<i>H. sarcophaga</i>	0.66

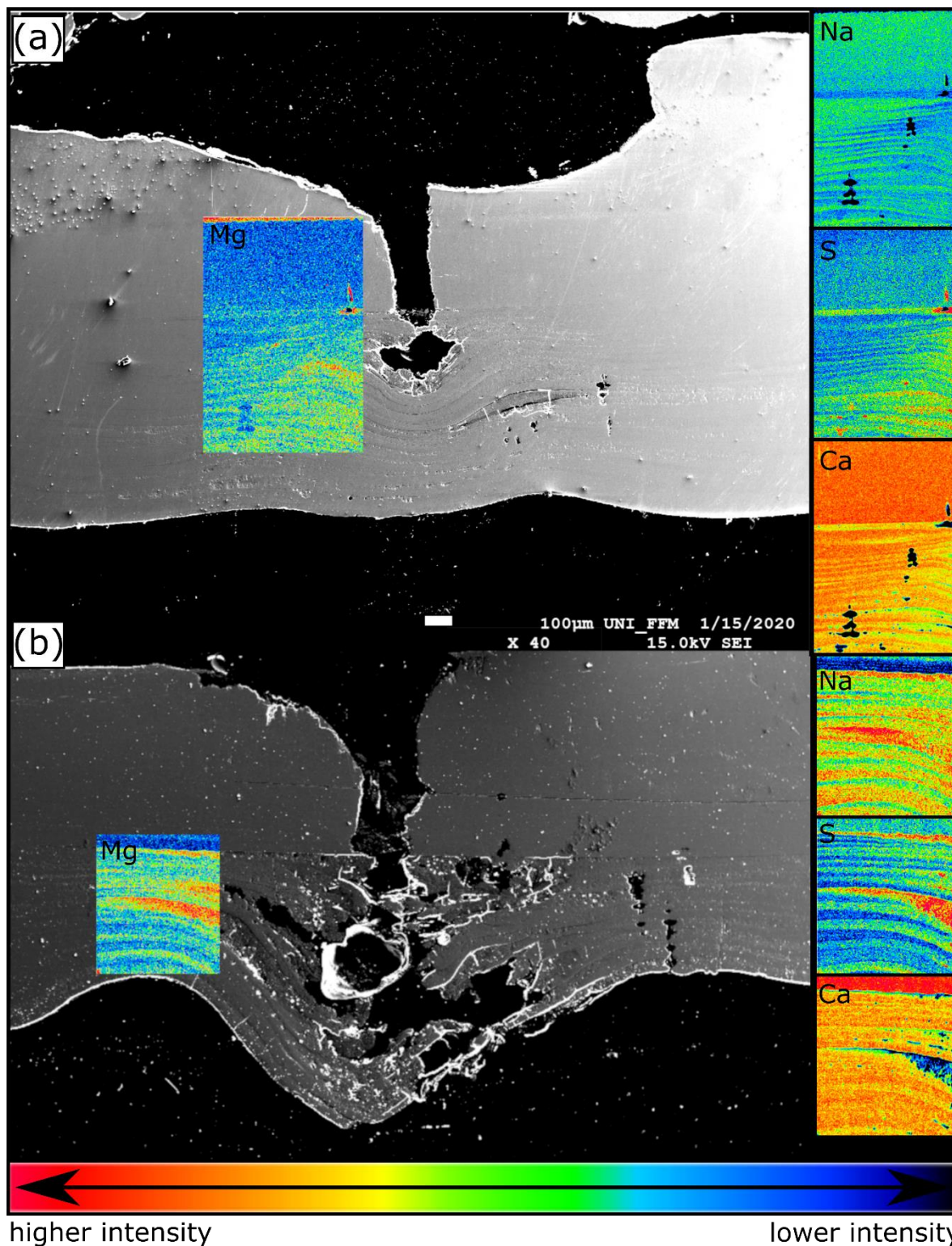
234

235 Within the bivalve shell Mg/Ca varies between 0.2 and 13.7 mmol mol⁻¹ (Fig. 2). Lowest values were
 236 found in the aragonitic shell layer (Fig 1/E₃) and highest values are measured in the microgranular
 237 calcitic shell layer (Fig 1/E₂). The highest Mg/Ca ratios are measured in the foraminiferal calcite (mean
 238 = 45.0 ± 17.9 mmol mol⁻¹, max = 80.6 mmol mol⁻¹).

239 Na/Ca ratio are characterized by similar values in the different sections when considering the
 240 carbonate polymorph, that they are built of. The aragonitic sections (Fig 1/E₃), bivalve aragonite and
 241 SRZ, have mean Na/Ca ratios of 22.0 ± 2.3 mmol mol⁻¹ (mean ± sd) and 25.3 ± 3.8 mmol mol⁻¹
 242 respectively. The SRZ displays a higher variability than the undisturbed aragonite. The microgranular
 243 calcite is characterised by a mean Na/Ca of 14.8 ± SD = 3.7 mmol mol⁻¹ (Fig 1/E₂).

244 The SRZ is enriched in Sr/Ca compared to the undisturbed shell sections. Mean ratios are nearly four
 245 times higher than in the undisturbed aragonitic shell parts (5.9 ± 2.1 mmol mol⁻¹ compared to 1.5 ± 0.2
 246 mmol mol⁻¹). Lowest values are measured in the bivalve's microgranular calcite (mean = 0.9 ± 0.1 mmol
 247 mol⁻¹).

248 S/Ca ratios are comparable in the undisturbed bivalve aragonite and microgranular calcite, with 1.9 ±
 249 0.3 mmol mol⁻¹ and 2.1 mmol mol⁻¹ ± 0.8 mmol mol⁻¹, respectively. Similar to Sr/Ca, the highest mean
 250 and maximum S/Ca ratios are measured in the SRZ (mean = 3.8 ± 2.5 mmol mol⁻¹, max = 11.1 mmol
 251 mol⁻¹. However, all these differences are insignificant (Table 1).

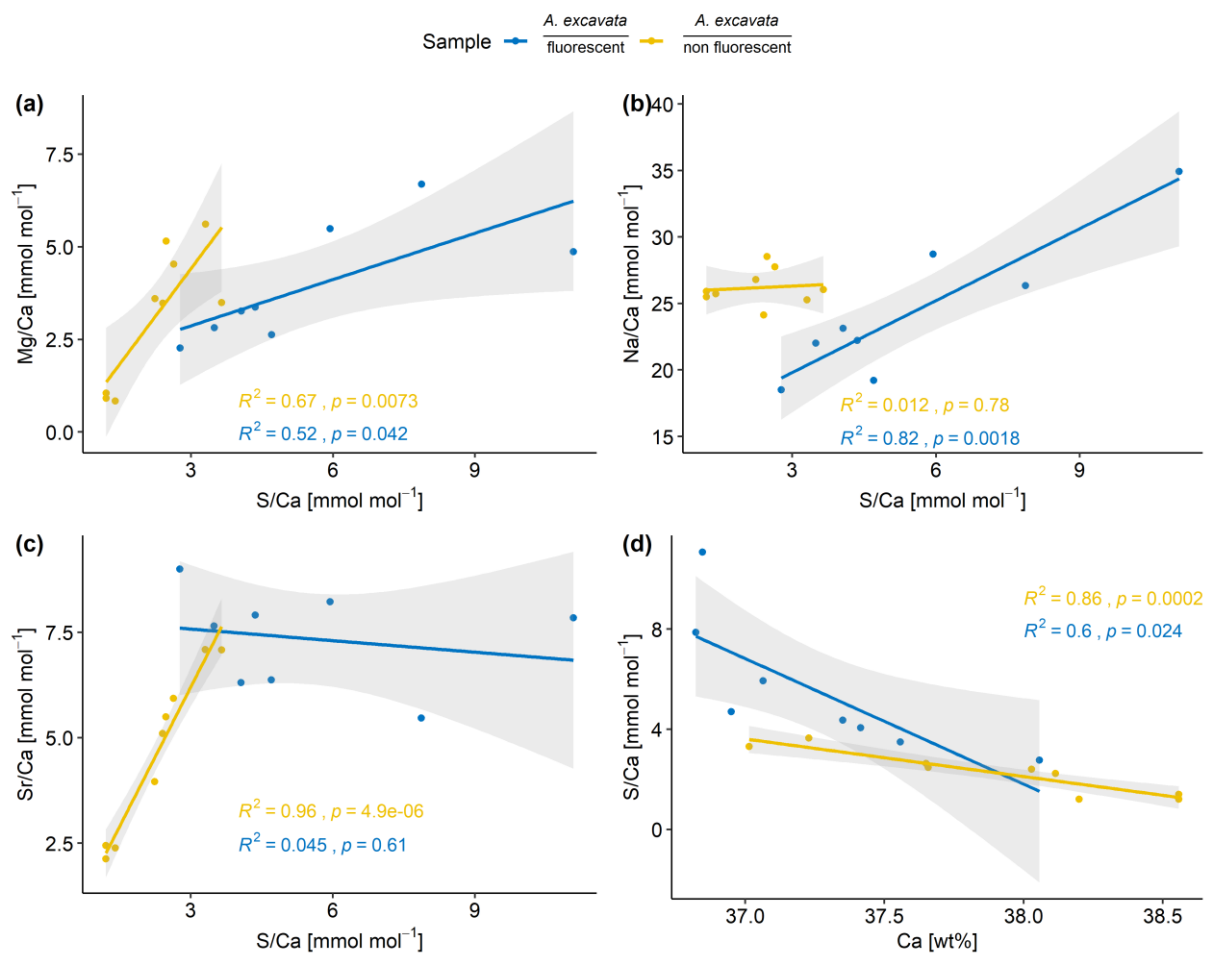


253 higher intensity lower intensity

254 Figure 3 EPMA element maps and secondary-electron image from an SEM of the callus area of two specimen (A & B) of *A.*
 255 *excavata*. Intensity scale in counts per second (cps). Min-Max counts amount to: Mg (10-24 cps), Na (76-132 cps) Ca (7600-
 256 8650 cps), S (8.5-33)

257 As also visible in the fluorescence image (Fig. 1), the EPMA chemical maps show a layering pattern (Fig.
 258 3). Highly fluorescent layers, that coincide with Mg and S maxima and Ca minima are variable in size

259 ranging from 15 to 80 μm in thickness. Non-fluorescent layers that coincide with Mg and S minima and
 260 Ca maxima are more uniform in size, ranging from 12.5 to 30 μm in thickness. Mean composition of
 261 the fluorescent (fl) and non-fluorescent (nfl) layers, based on EPMA point measurements amount to:
 262 fl: Mg/Ca = $3.8 \text{ mmol mol}^{-1} \pm 1.7 \text{ mmol mol}^{-1}$, Sr/Ca = $7.4 \text{ mmol mol}^{-1} \pm 1.2 \text{ mmol mol}^{-1}$, Na/Ca = 24.4
 263 $\text{mmol mol}^{-1} \pm 5.4 \text{ mmol mol}^{-1}$, S/Ca = $5.5 \text{ mmol mol}^{-1} \pm 2.7 \text{ mmol mol}^{-1}$; nfl: Mg/Ca = $3.2 \text{ mmol mol}^{-1} \pm$
 264 $1.8 \text{ mmol mol}^{-1}$, Sr/Ca = $4.6 \text{ mmol mol}^{-1} \pm 1.9 \text{ mmol mol}^{-1}$, Na/Ca = $26.6 \text{ mmol mol}^{-1} \pm 1.3 \text{ mmol mol}^{-1}$,
 265 S/Ca = $2.3 \text{ mmol mol}^{-1} \pm 0.9 \text{ mmol mol}^{-1}$. Significant mean differences between fluorescent and non-
 266 fluorescent layers, based on Wilcoxon-Mann-Whitney test, are evident with regards to the S/Ca
 267 ($p < 0.001$) and Sr/Ca ratios ($p = 0.006$).



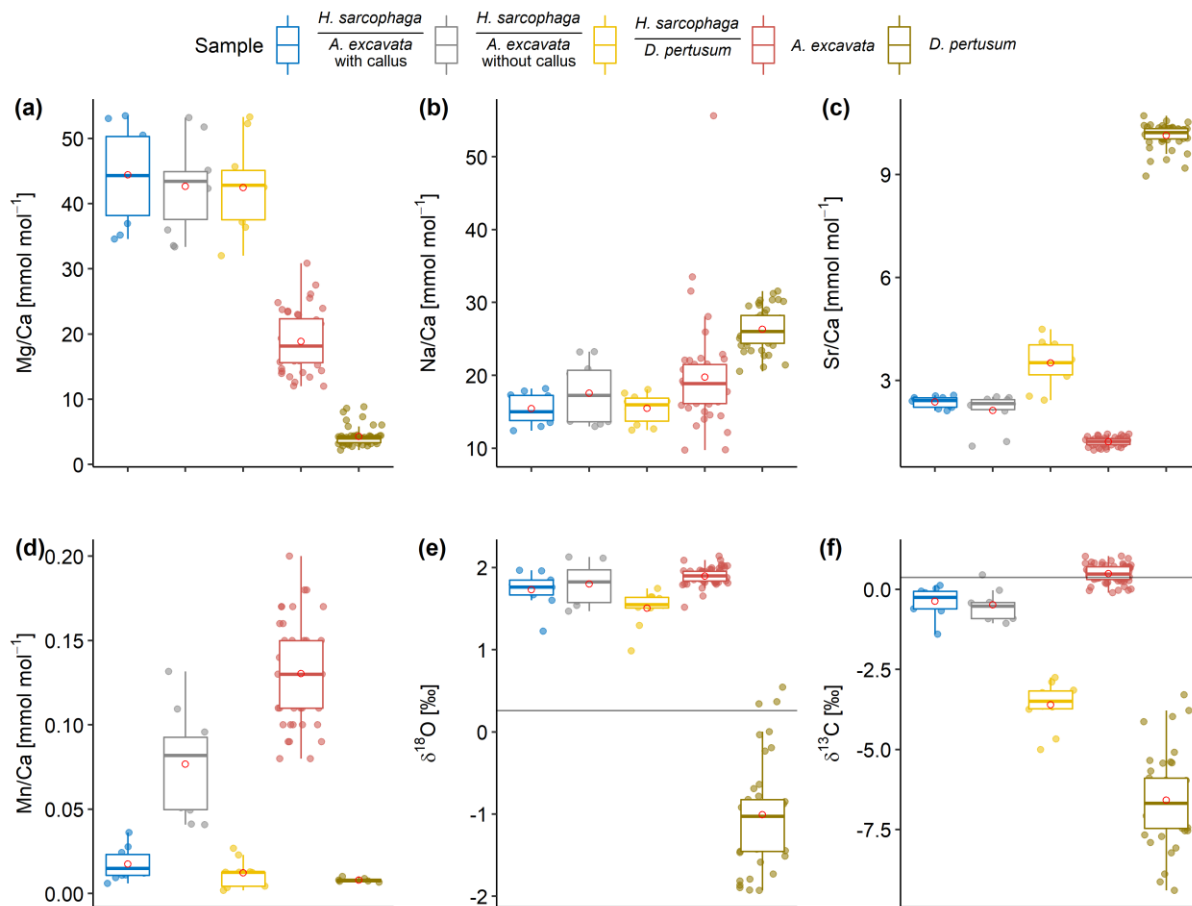
268

269 Figure 4 Elemental composition of the SRZ divided according to their fluorescence. Linear correlations are shown for both
 270 layers with 95% confidence intervals in gray. Correlations are calculated with a linear regression model with OLS.

271 Mg/Ca and S/Ca as well as Na/Ca and S/Ca display significant correlations in the fluorescent layers
 272 (Fig. 4). In the non-fluorescent shell layers, Mg/Ca and S/Ca, Sr/Ca and S/Ca are significantly
 273 correlated. In both layers, S/Ca ratios are inverse correlated with Ca wt% (Fig. 4).

274

275

277 **3.4. Stable carbon and oxygen isotope**

278

279 Figure 5 Box- and whisker plots displaying the E/Ca (ICP-OES and ICP-MS) and stable isotope analysis (MS) of the investigated
 280 specimens. Boxes display the interquartile range and lines the median values. The whiskers show min and max values that
 281 are within the range of $Q1 - 1.5 \cdot IQR - Q3 + 1.5 \cdot IQR$. Red circles show mean values. Lines in E and F show the isotopic
 282 composition of the ambient seawater. Text below the horizontal lines in the legend is the host organism that *H. sarcophaga*
 283 grew on.

284 The different *H. sarcophaga* shells exhibit differences in their isotopic composition based on their host
 285 organism (Fig. 4 E/F). In particular, $\delta^{18}\text{O}$ values are similar in HL and HA with $+1.51 \pm 0.22 \text{ ‰}$ and $+1.80$
 286 $\pm 0.25 \text{ ‰}$, respectively. These values are in accordance with $\delta^{18}\text{O}$ values from the host organism *A.*
 287 *excavata*, which range from $+1.52 \text{ ‰}$ to $+2.1 \text{ ‰}$. *D. pertusum* displays more depleted $\delta^{18}\text{O}$ and $\delta^{13}\text{C}$
 288 values, ranging from -1.93 ‰ to $+0.54 \text{ ‰}$ and -9.41 ‰ to -3.30 ‰ .

289 Larger differences between the different *H. sarcophaga* samples are observable in the carbon isotopic
 290 signature of specimens taken from different host organisms. HA display $\delta^{13}\text{C}$ values of $-0.43 \pm 0.47 \text{ ‰}$
 291 which is close to the ratios of their host organism, being $+0.49 \pm 0.28 \text{ ‰}$. HL are more depleted in heavy
 292 carbon isotopes with a measured value of $-3.61 \pm 0.71 \text{ ‰}$. For reference, the isotopic composition of
 293 the ambient seawater is $\delta^{18}\text{O} = +0.26 \text{ ‰}$ and $\delta^{13}\text{C} = +0.38 \text{ ‰}$.

294 The isotopic composition of HAW and HAO can be described by linear functions whereas the isotopic
 295 composition in HL cannot:

$$296 \delta^{13}\text{C}_{\text{HAW}} = 1.8 \pm 0.4 * \delta^{18}\text{O} - 3.4 \pm 0.8 (r^2 = 0.7, p=0.004, df = 7) \quad [1]$$

$$297 \delta^{13}\text{C}_{\text{HAO}} = 1.1 \pm 0.3 * \delta^{18}\text{O} - 2.6 \pm 0.6 (r^2 = 0.6, p=0.02, df = 6) \quad [2]$$

$$298 \delta^{13}\text{C}_{\text{HL}} = 1.7 \pm 1.0 * \delta^{18}\text{O} - 6.2 \pm 1.5 (r^2 = 0.18, p=0.12, df = 8) \quad [3]$$

299 3.5. ICP-OES results from *H. sarcophaga* grown on different host organisms

300 *H. sarcophaga* samples from different host organisms are similar in their chemical composition with
 301 regard to Mg/Ca and Na/Ca (Fig. 5 A/B). Mean Mg/Ca ratios range from 42.7 ± 6.8 to 44.4 ± 7.2 mmol
 302 mol⁻¹. Both host organisms have lower mean Mg/Ca ratios of 4.3 ± 1.5 mmol mol⁻¹ and 18.9 ± 4.5 mmol
 303 mol⁻¹ in *D. pertusum* and *A. excavata*, respectively.

304 Mean Na/Ca ratios range between 15.4 ± 2.1 to 17.6 ± 4.3 mmol mol⁻¹ for *H. sarcophaga*. The highest
 305 Na/Ca ratios and variations are measured in HAO. *D. pertusum* displays overall higher Na/Ca ratios
 306 than *H. sarcophaga* (26.3 ± 2.8 mmol mol⁻¹). The highest variation is measured in *A. excavata* ranging
 307 from 9.8 to 55.6 mmol mol⁻¹ with a mean of 19.8 ± 7.3 mmol mol⁻¹.

308 A clear difference in Sr/Ca of 1.1 ± 0.16 mmol mol⁻¹ is evident between *H. sarcophaga* from the
 309 different host organisms (Fig. 5 C). HAW and HAO show mean Sr/Ca ratios of 2.4 ± 0.2 and 2.1 ± 0.5
 310 mmol mol⁻¹, respectively. The host organism *A. excavata* has lower Sr/Ca ratios (1.2 ± 0.1 mmol mol⁻¹).
 311 On the contrary, HL and *D. pertusum*, display higher mean Sr/Ca ratios of 3.5 ± 0.7 and 10.13 ± 0.3
 312 mmol mol⁻¹ respectively.

313 Prominent differences between *H. sarcophaga* groups are also evident in their Mn/Ca ratios (Fig. 5 D).
 314 HAW, HL and *D. pertusum* display Mn/Ca ratios of 0.017 ± 0.01 mmol mol⁻¹, 0.012 ± 0.008 mmol mol⁻¹
 315 and 0.008 ± 0.001 mmol mol⁻¹, whereas HAO and *A. excavata* show higher Mn/Ca ratios of 0.077 ± 0.03
 316 mmol mol⁻¹ and 0.13 ± 0.03 mmol mol⁻¹, respectively.

317 3.6. Compositional differences in *H. sarcophaga* related to their host organism

318 Table 2 Results of the one-way ANOVA and Kruskal-Wallis analysis with the host organism as predictor variable. Bold fields
 319 show elemental and isotopic ratios in *H. sarcophaga* that may be significantly influenced by the chemistry of the host
 320 organism. *p*-values are Bonferroni adjusted.

	ANOVA					
	Mg/Ca	Na/Ca	Sr/Ca	Mn/Ca	$\delta^{18}\text{O}$	$\delta^{13}\text{C}$
DFn	2					
DFd	25					
F	0.2	0.22	23	32	4.1	97
<i>p</i>	0.82	0.8	<0.001	<0.001	0.029	<0.001
Generalized eta squared	0.015	0.018	0.65	0.74	0.26	0.89

Kruskal-Wallis test						
n	28					
df	2					
p	0.83	0.92	<0.001	<0.001	0.03	<0.001

321

322 We conducted a one-way ANOVA and Kruskal-Wallis test (Table 2) in order to explore if the
 323 investigated *H. sarcophaga* groups (HAW, HAO, HL) show significant differences in their geochemical
 324 composition related to their host organism. We used the measured elemental and isotopic
 325 composition as target variables and the host organisms (*A. excavata* with callus, *A. excavata* without
 326 callus, *D. pertusum*) as the factor variable. Tukey-HSD (Table 3) was used as post-hoc test to investigate
 327 group specific mean differences.

328 Table 3 Tukey-HSD test results. Bold fields show significant differences between the two groups. HAW = *H. sarcophaga* that
 329 infested *A. excavata* with callus formation, HAO = *H. sarcophaga* that infested *A. excavata* without callus formation, HL = *H.*
 330 *sarcophaga* that infested *D. pertusum*. *p*-values are Bonferroni adjusted.

Tukey-HSD test				
	Group 1	Group 2	Difference	<i>p</i>
Mg/Ca	HAW	HAO	-1.22	0.93
	HAW	HL	-1.95	0.81
	HAO	HL	-0.73	0.97
Na/Ca	HAW	HAO	0.74	0.81
	HAW	HL	0.05	0.99
	HAO	HL	-0.68	0.84
Sr/Ca	HAW	HAO	-0.004	1
	HAW	HL	1.14	<0.001
	HAO	HL	1.14	<0.001
Mn/Ca	HAW	HAO	0.05	<0.001
	HAW	HL	-0.005	0.75
	HAO	HL	-0.05	<0.001
$\delta^{18}\text{O}$	HAW	HAO	0.07	0.81
	HAW	HL	-0.23	0.11
	HAO	HL	-0.30	0.032
$\delta^{13}\text{C}$	HAW	HAO	-0.11	0.91
	HAW	HL	-3.24	<0.001
	HAO	HL	-3.12	<0.001

331

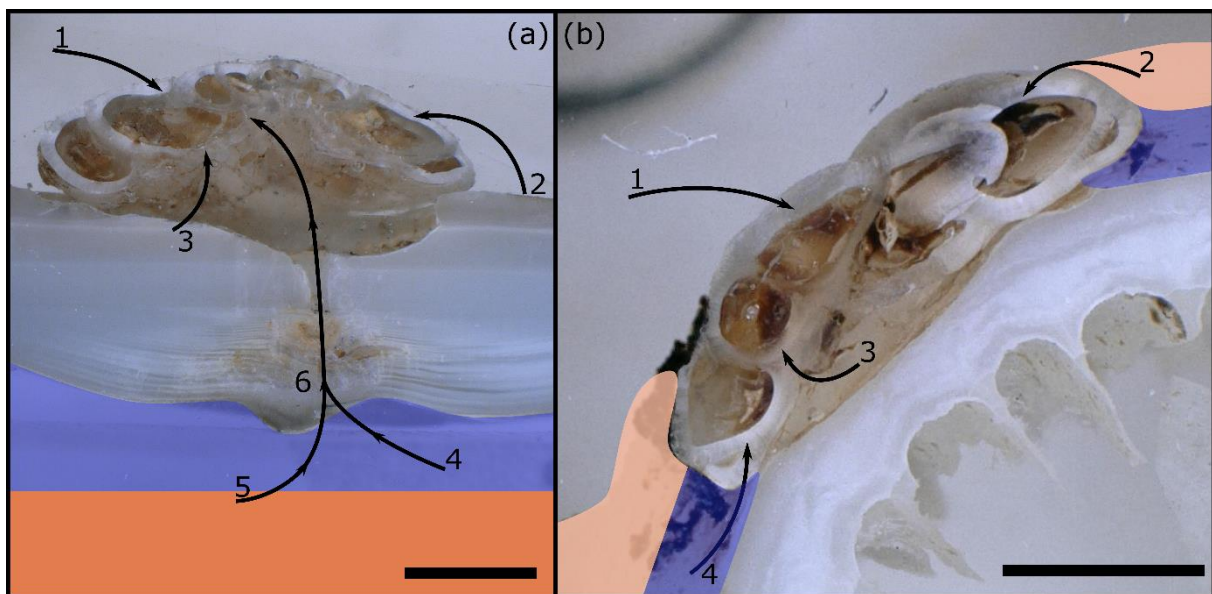
332 The one-way ANOVA reveals no significant difference in the Mg/Ca and Na/Ca ratios of the
 333 foraminifera that were collected from the different host organisms (Table 2). In contrast, the ANOVA
 334 suggests a significant difference between Sr/Ca and Mn/Ca ratios between these two groups. In the
 335 case of Sr/Ca, significant differences based on the Tukey-HSD post-hoc test are observable between
 336 HL and HA, whereas we find no significant differences between HAW and HAO. In addition, we observe
 337 no significant differences between HAW and HL in their Mn/Ca composition, but significant differences
 338 are present between both these groups and HAO.

339 In the case of the stable oxygen isotope composition, we observe significant differences between *H.*
340 *sarcophaga* specimens from different host organisms. The $\delta^{18}\text{O}$ measured in HL is significantly lower
341 than in HAO. Significant differences are also observable for $\delta^{13}\text{C}$ ratios. Here, differences in the isotopic
342 composition are detectable between HL and HA, with the latter showing higher $\delta^{13}\text{C}$ ratio.

343 The Kruskal-Wallis test, which was used as a non-parametric cross validation for the ANOVA test, shows
344 the same results as the ANOVA test

345 4. Discussion

346 4.1. Mechanisms of etching and boring



347
348 Figure 6 Possible pathways of E/Ca and isotopic signals into the foraminiferal calcite.
349 A: *H. sarcophaga* on *A. excavata*, B: *H. sarcophaga* on *D. pertusum*. Blue areas represent the calcifying space, orange areas
350 represent mantle tissue in *A. excavata* (A) and organic layer (coenosarc/mucus) in *D. pertusum* (B). Uptake of seawater and
351 free-floating particles (1), Ingestion of host organic material (periostracum, coral tissue/mucus) (2), Ingestion of dissolved
352 carbonate material (3), Ingestion of extracellular calcifying fluid (ECF) (4), Ingestion of Mantle tissue (5), ingestion
353 of carbonate and organic material from the deposited callus (6). Scalebar is 100 μm . Please note that the calcifying space and
354 organic layers are displayed enlarged for improved visibility. Actual size of the calcifying space amounts to 1-100 nm
355 (Nakahara, 1991; Tambutté et al., 2007). The organic layer (coenosarc) is $\sim 25 \mu\text{m}$ in thickness (Tambutté et al., 2007).

356 The boring and etching of *H. sarcophaga* in *A. excavata* and *D. pertusum* can serve multiple purposes.
357 The attachment etchings of foraminifera have been proposed to serve as an anchoring function and
358 increase protection from predators and the hydrodynamic regime. Possibly, the foraminifera also
359 dissolve the host's carbonate material to satisfy the calcium and/or DIC requirements of *H. sarcophaga*
360 for the calcification of its shell (Cedhagen, 1994; Véneç-Peyré, 1996; Todd, 1965), rather than
361 expending further energy to source Ca/DIC from the surrounding seawater (Fig 6A).

362 The boring in *A. excavata* is presumably produced to access the softbody of the bivalve, indicated by
363 the mantle damage in the vicinity of the boring (Cedhagen, 1994). Additionally, the foraminifera may
364 benefit from ingesting the ECF of the bivalve, containing carbohydrates, proteins, glycoproteins and

365 amino acids therefore constituting a valuable nutrient source (Yin et al., 2005). The ECF is also enriched
366 in Ca and CO₂ compared to the ambient seawater, maybe providing additional ions for the calcification
367 of *H. sarcophaga* (Crenshaw, 1972). Feeding on mantle fluids of bivalves by parasitic foraminifera is
368 also supported by tracer experiments on *C. refulgens* (Alexander and Delaca, 1987). With *D. pertusum*
369 as host, the foraminifera can access the coenosarc and underlying calcifying space of the coral without
370 having to bore through the carbonate skeleton (Fig. 6B).

371 *H. sarcophaga* probably uses chemical etching, as indicated by the xenoglyph surface texture of the
372 trace that changes in correlation with the host's microstructure (Beuck et al., 2008; Todd, 1965) A
373 possible mechanism was investigated in the non-symbiotic benthic foraminifera *Ammonia* sp., which
374 uses H⁺-ATPase to actively pump H⁺-ions out of their protoplasm to facilitate calcification (Toyofuku et
375 al., 2017). This proton-flux causes a pH decrease by up to 1.1 in a 100 μm wide zone around the
376 foraminifera (Toyofuku et al., 2017). Similar effects are reported from excavating sponges. *Cliona*
377 *varians* displays pH values as low as 5 in their filopodia during carbonate dissolution (Webb et al.,
378 2019).

379

380 **4.2. Sr/Ca differences in *H. sarcophaga* related to the host organism**

381 We observe significant differences in the Sr/Ca and Mn/Ca composition between *H. sarcophaga* from
382 different host organisms.

383 HL show significantly higher Sr/Ca ratios than HA. Given that this result is based on measurements
384 from multiple individuals distributed across more than one host organism, we suggest that this is most
385 likely a signal of the high Sr/Ca aragonite precipitated from *D. pertusum* that is imprinted into the test
386 of *H. sarcophaga*. By chemically corroding the attachment etching as well as by the penetrating boring
387 and by taking up the resulting solutions, the foraminifera gains access to a pre-concentrated calcium
388 carbonate solution from which it can precipitate its shell (Fig. 6). Naturally, the foraminifera would also
389 reflect other characteristics of the host, such as the high Sr/Ca ratio from the aragonite of *D. pertusum*
390 (Raddatz et al., 2013; Schleinkofer et al., 2019). In agreement with the much lower Sr/Ca ratios in
391 calcite and aragonite in *A. excavata* (Schleinkofer et al., 2021) compared to the coralline aragonite, we
392 do not observe such high Sr/Ca ratios in HA. Still, the observed Sr/Ca ratios in HA are higher by a factor
393 of two than in the host organism. Since we do not observe differences between HAW and HAO, the
394 Sr/Ca surplus cannot be derived from the ingestion of organic material from within the shell cavity. We
395 hypothesize that a possible further control is likely provided through the mixture of dissolved host
396 CaCO₃ material and ambient seawater from which the foraminifera calcify, which is explored in more
397 detail in the next section.

398 **4.3. Mixing model**

399 In order to further investigate the observed results, we created a simple two-component model to
 400 explore how the trace-element chemistry of *H. sarcophaga* could change by delivery of ions to the
 401 calcification site that were derived from dissolution of the host organism. In this model we calculate
 402 changes of the foraminifera composition in dependence from an assumed calcification from a variable
 403 mixture of seawater and dissolved host carbonate material. We excluded the addition of the hosts
 404 calcifying fluid in the model because there is no data available for the chemical composition of the
 405 calcifying fluid of *D. pertusum* nor *A. excavata*, and because the model is intended only as an initial
 406 exploration of whether the geochemistry of *H. sarcophaga* can be explained by calcification from a
 407 mixture of seawater and dissolved host material. Furthermore, measurements of the chemical
 408 composition of the calcifying fluid of other bivalve species indicate that the composition is close to the
 409 composition of seawater (Wada and Fujinuki, 1976; Crenshaw, 1972).

410 The model calculates element/Ca ratios based on calcite precipitation from a fluid that is derived from
 411 a mix of seawater (transported to the calcification site, see e.g., (Erez, 2003)), and CaCO₃ dissolved
 412 from the host organism:

$$413 \frac{E}{Ca_{Hydrokin}} = \frac{E_{SW} + \frac{10^R}{M_{Carb}} * \frac{E}{Ca_{Host}}}{Ca_{SW} + \frac{10^R}{M_{Carb}}} * D_E * 1000 \quad [4]$$

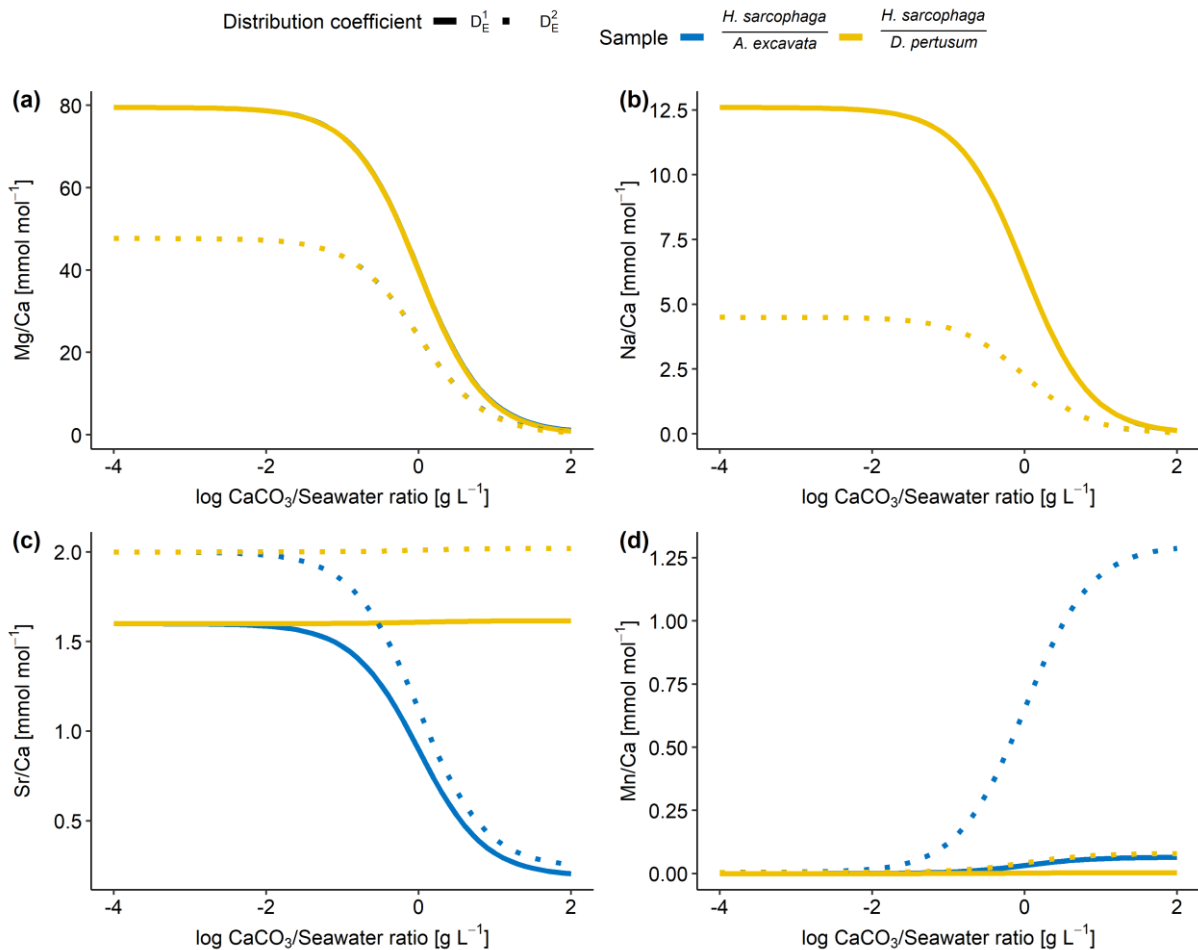
414 Where E_{SW} = element concentration in seawater, E/Ca_{Host} = element/Ca in host carbonate [mmol mol⁻¹],
 415 Ca_{SW} = Calcium concentration in seawater (0.010 mol L⁻¹), D_E = Calcite-Water distribution coefficient,
 416 M_{Carb} = atomic mass of CaCO₃ (100.08 g mol⁻¹) and R = log mixing ratio between carbonate and seawater
 417 [g L⁻¹].

418 Table 4 Parameters used in the proposed model to explore the effects of carbonate and water uptake of *H. sarcophaga* on
 419 the shell chemistry. Host element/Ca ratios are derived from this study. D_E¹ & D_E² = Distribution coefficient

Model parameters					
	E _{SW} [mol L ⁻¹]	E/Ca _{Acesta} [mmol mol ⁻¹]	E/Ca _{Desmophyllum} [mmol mol ⁻¹]	D _E ¹	D _E ²
Mg	0.053	19	4.2	0.015 (Segev and Erez, 2006)	0.009 (Oomori et al., 1987)
Na	0.450	20	26	0.00028 (Evans et al., 2015)	0.0001 (Füger et al., 2019)
Sr	0.0001	1.2	10.1	0.16 (Raitzsch et al., 2010)	0.2 (Mucci and Morse, 1983; Evans et al., 2015)
Mn	5*10 ⁻⁹	0.131	0.008	0.5	10 (Mucci, 1988)

420

421 As we have no information about the amount of dissolved material and water that is taken up by *H.*
422 *sarcophaga*, we modelled it over six orders of magnitude (log dissolved CaCO_3 /seawater ratios of -4 to
423 +2). The parameters used are reported in Table 4.



424

425 Figure 7 Results of model calculations with the parameters listed in Tab. 4 for the measured E/Ca ratios. Text below the
426 horizontal lines in the legend is the host organism that *H. sarcophaga* grew on. Independently of the mixing ratio of dissolved
427 host CaCO_3 and ambient water, no differences of the geochemical signature is predictable in Mg/Ca and Na/Ca. On the
428 contrary, Sr/Ca and Mn/Ca ratios are predicted to diverge at mixing ratios $> 0.01 \text{ g CaCO}_3 \text{ L}^{-1}$ seawater. Solid lines are produced
429 with D_E^1 for the calculation and dotted lines are produced with D_E^2 for the calculation (see Tab. 4). In panel a and b, the
430 different samples overlap each other.

431 Based on the model shown in Fig. 7, the Mg/Ca and Na/Ca ratios in *H. sarcophaga* are independent of
432 the geochemical signature of the host it lived on, which is in agreement with our measurements. This
433 is caused by the high concentration of these elements in the ambient seawater in comparison to the
434 host's carbonate. The composition of the mixture is largely controlled by the addition of Ca, which is
435 equal for both host organisms.

436 In contrast, the model predicts that, at high ratios of CaCO₃ derived from the host compared to the
437 surrounding seawater, different Sr/Ca and Mn/Ca ratios should be observed between foraminifera
438 living on different host organisms. The modelled Sr/Ca ratios for HL are constant at 2.0 mmol mol⁻¹
439 independent from the mixing ratio (Fig. 7C). When the foraminifera dissolves aragonitic material of *D.*
440 *pertusum* and this material is mixed with seawater, the resulting Sr/Ca ratios in this solution do not
441 change due to the aragonitic D_{Sr} being close to 1. Consequently, if the shell Sr/Ca ratio in *H. sarcophaga*
442 depends on calcite D_{Sr} and the Sr/Ca ratio in the calcifying fluid of *H. sarcophaga*, the resulting Sr/Ca
443 ratio in HL is equivalent to a specimen that calcifies solely from seawater (specimen without a host).
444 As the calcitic D_{Sr} is below 1 (Raitzsch et al., 2010; Mucci and Morse, 1983; Evans et al., 2015), the
445 addition of dissolved material from *A. excavata* in the calcifying space results in decreasing Sr/Ca ratios
446 in the calcifying fluid and lower Sr/Ca ratios in the precipitated calcite of the foraminifera. Similar
447 results are obtained in the case of Mn/Ca ratios. The addition of dissolved host material to the
448 calcifying space of *H. sarcophaga* results in an increase of the Mn/Ca ratio in the calcifying fluid, which
449 leads to increasing Mn/Ca ratios in the foraminiferal calcite.

450 The proposed model can help us understand why we do not see changes in the Mg/Ca and Na/Ca
451 composition of *H. sarcophaga* from different host organisms and why Sr/Ca and Mn/Ca ratios differ
452 between these groups (Fig. 2). Nonetheless, other processes are clearly required to explain the details
453 of trace element uptake in *H. sarcophaga*. Sr/Ca ratios in HL, for instance, can only be modelled up to
454 2 mmol mol⁻¹, whereas we measure a mean of 3.5 mmol mol⁻¹. The results of this model are largely
455 driven by the distribution coefficients used, however, the distribution coefficients used in this model
456 are not empirically determined on *H. sarcophaga* but derive from other foraminifera species (D_E¹) or
457 inorganic precipitation experiments (D_E²). The model does also not account for growth-rate driven
458 differences in trace element partitioning, while this is especially relevant in the case of Na and Mn
459 (Mucci, 1988; Füger et al., 2019). In addition, we have to consider lattice strain-effects that increase
460 the distribution coefficient for other elements such as Sr and Na, as *H. sarcophaga* has relatively high
461 concentrations of Mg (Evans et al., 2015; Mucci and Morse, 1983).

462 As discussed above, this is a simplified model that uses seawater and dissolved carbonate as
463 endmembers. An additional possibility is that the foraminifera pumps or channels ions into and out of
464 the calcifying fluid. In particular, it has been suggested foraminifera are able to transport Mg out of
465 the calcifying space (Nehrke et al., 2013; Toyofuku et al., 2017; Bentov and Erez, 2006), but
466 intermediate and high-Mg foraminifera such as *A. lessonii* appear to exert a lower degree of control
467 over the composition of their calcifying fluid compared to low-Mg species (Evans et al., 2018; Geerken
468 et al., 2018). Assuming the calcifying fluid is depleted in Mg in comparison to seawater, the model

469 would predict lower Mg/Ca ratios, although importantly, it would still not predict a difference in the
470 Mg/Ca ratios of *H. sarcophaga* influenced by the host organism.

471 Another factor that should be considered is the transport pathway of the dissolved material into the
472 foraminifera's calcifying fluid. The dissolution process of the host organism could modify the chemistry
473 of the ambient seawater in a limited area around the foraminifera (Toyofuku et al., 2017), although
474 this process is hard to imagine in an environment (cold-water coral reef) that relies on constant water
475 movement to provide nutrients to the main inhabitants (Mienis et al., 2007). As such, we suggest it is
476 more likely, that the dissolved material is transported through the cytoplasm to the calcification site
477 (Spero, 1988; Erez, 2003), although further work is required to confirm this.

478 **4.4. Mn/Ca differences in *H. sarcophaga* related to the host organism**

479 Based on the ANOVA analysis (Table 2), significant differences are also observable in the Mn/Ca ratios.
480 HAO display four times higher Mn/Ca ratios than in the other two observed groups. HL show similar
481 Mn/Ca ratios as their host organism, both HAW and HAO show lower Mn/Ca ratios. Based on the
482 differences we observe between the samples that were picked from *A. excavata*, it is unlikely that the
483 Mn/Ca signal in *H. sarcophaga* derives from the host shell material (Fig. 6/A3 & B3). In this case we
484 would expect to see differences between HA and HL as Mn/Ca in *A. excavata* is approximately one
485 order of magnitude higher than in *D. pertusum*. Influences of the surrounding water cannot explain
486 the observed differences either. Manganese, as a redox-sensitive element, is controlled by the oxygen
487 concentration of the ambient water. Under well oxygenated conditions, the main species Mn^{2+} is
488 oxidized to Mn-oxyhydroxides and precipitated (Calvert and Pedersen, 1996, 1993). Low-oxygen
489 conditions lead to a reduction of Mn-oxyhydroxides to the bioavailable Mn^{2+} and a consequent
490 increase of Mn/Ca ratios in biogenic carbonates (Tribovillard et al., 2006; Groeneveld and Filipsson,
491 2013; Koho et al., 2015). The Leksa Reef, however, is well oxygenated (Milzer et al., 2013; Jacobson,
492 1983).

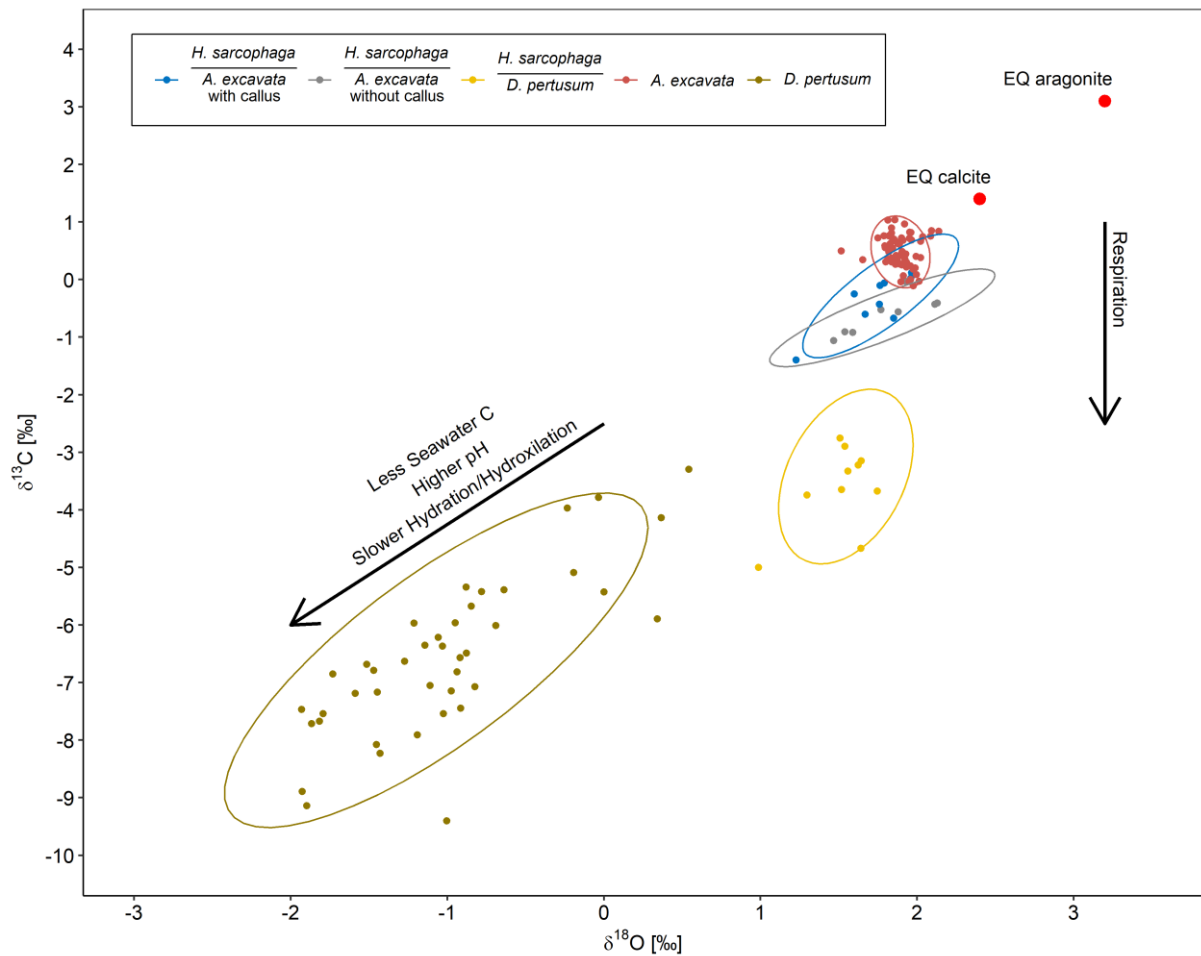
493 An influence of the precipitation rate on Mn/Ca ratio was shown in inorganically precipitated calcite
494 overgrowths and the planktic foraminifera *Orbulina universa* (Mucci, 1988; Lorens, 1981; Holland et
495 al., 2017). Generally speaking, increased calcification rates cause Mn/Ca ratios in the precipitates to
496 decrease (Mucci, 1988; Holland et al., 2017). In our investigated samples, this effect would imply lower
497 calcification rates in HAO compared to HAW and HL. The possibility of HAO having low calcification
498 rates is likely, as it is missing a valuable nutrient source (Fig. 6). Due to the high distribution coefficient
499 of manganese, Rayleigh fractionation might add an additional control on Mn/Ca ratios in the
500 foraminifera shell (Holland et al., 2017). The model of Rayleigh fractionation relies on a number of
501 assumptions about the internal reservoir of the foraminifera regarding the size, initial composition,

502 refreshment rate and calcification rate (Elderfield, 1996). As these parameters are not fully
503 understood, both for *H. sarcophaga* and foraminifera in general, we cannot provide further
504 information about the possible influence.

505 A significant influence of the potentially Mn-enriched bodily fluids of bivalves (Wada and Fujinuki,
506 1976) also cannot explain the differences in the chemical composition as the samples that discern from
507 the others are picked from HAO. These foraminifera did not have access to the internal organic
508 material of the bivalve (Fig. 6/A4). Instead, the high Mn signal in HAO must derive from a source that
509 is located on the outside of the bivalve host (Fig. 6/A2). When the foraminifera initially infests the
510 bivalve and starts boring into the shell, nutrient sources other than the internal organic parts of the
511 bivalve have to be utilised by *H. sarcophaga*. The organic periostracum of the bivalve could depict this
512 nutrient source as it is a highly nutritional source for organic material on the outside of the bivalve's
513 shell (Secor et al., 1993). High concentrations of Mn and Fe were measured in the periostracum of
514 freshwater and marine bivalves (Swinehart and Smith, 1979; Allen, 1960). The mechanistic explanation
515 for this enrichment of Mn and Fe is reported to be the high amount of the amino acids containing
516 glycine and tyrosin in the periostracum of bivalves (Piez, 1961; Whitney et al., 2019), which act as
517 complexing sites for metal ions (Swinehart and Smith, 1979). The existence of living *H. sarcophaga*
518 attached to rocks demonstrates that they do not necessarily rely on a living host but can also supply
519 themselves through other feeding strategies (Cedhagen, 1994). Since algae take up Mn and
520 concentrate it internally (Sunda and Huntsman, 1985), the increased Mn/Ca in HAO could also be
521 caused by a facultative suspension feeding mode of *H. sarcophaga* during its juvenile stage.

522 At this point we can only speculate about the mechanistic explanation for the enrichment of Mn/Ca in
523 HAO. Future research on *H. sarcophaga* should involve spatially resolved Mn and Fe measurements,
524 to explore if there is an ontogenetic decrease of Mn/Ca ratios in the test of *H. sarcophaga* picked from
525 *A. excavata*. This decrease would mark the time of the first penetration of the bivalve shell.

526 **4.5. Carbonate isotopic composition in *H. sarcophaga* based on the host organism**



527

528 Figure 8 $\delta^{18}\text{O}$ plotted against $\delta^{13}\text{C}$ for *H. sarcophaga* from different host organisms and the host organisms *A. excavata* and
 529 *D. pertusum* with 95 % confidence ellipse. Arrows show compositional changes induced by kinetic effects and respiration.
 530 Text below the horizontal lines in the legend is the host organism that *H. sarcophaga* grew on. Red points show the
 531 equilibrium composition for calcite and aragonite as calculated from the isotopic composition of the ambient seawater.

532 The oxygen and carbon isotopic composition of the different organisms are characterised by large
 533 differences. *A. excavata* does not show signs of kinetic effects which would be indicated by a
 534 correlation of $\delta^{13}\text{C}$ and $\delta^{18}\text{O}$ values (McConnaughey, 2003; Adkins et al., 2003; Bajnai et al., 2018).
 535 Bivalves are largely considered to calcify in equilibrium with the surrounding water (Immenhauser et
 536 al., 2016), which appears to be valid for *A. excavata* as it displays an isotopic composition close to the
 537 expected equilibrium (Fig. 8). The host organism *D. pertusum* displays higher departures from the
 538 expected aragonite equilibrium, which is mainly caused by additional incorporation of isotopically
 539 lighter, metabolic CO_2 and by kinetic isotope effects associated with hydration/hydroxylation reactions
 540 given that this coral raises the calcification site pH to values significantly exceeding seawater pH (Chen
 541 et al., 2018; McCulloch et al., 2012).

542 Interestingly, the *HA* samples display an isotopic composition very similar to the composition of its
 543 host organism (Fig. 8). The 95 % confidence ellipsoids of HAW, HAO and *A. excavata* all overlap at
 544 highest $\delta^{18}\text{O}$ values. However, in contrast to *A. excavata*, HAW and HAO display positive correlations

545 between $\delta^{18}\text{O}$ and $\delta^{13}\text{C}$. This may indicate that all three organisms closely mineralize their carbon from
546 the same source, but hydration/hydroxylation kinetics occur more pronounced in HAW and HAO
547 relative to *A. excavata*.

548 The observable differences in the carbon isotopic composition between HA and HL can also be caused
549 by different proportions of the carbon sources. HL presumably have constant access to the host's
550 carbon pool, whereas the access of HA to the host's carbon pool is limited due to the defence
551 mechanism of *A. excavata* (Fig. 3). When the bivalve has successfully closed the boring of the
552 foraminifera, the foraminifera must use seawater DIC as a carbon source until it penetrates the shell
553 again. This mixing of different carbon sources in HA in contrast to the stable carbon source of HL can
554 explain the lower $\delta^{13}\text{C}$ values in HL due to an increased influence of host derived carbon.

555 HL is characterized by significantly more positive $\delta^{18}\text{O}$ values than its host, and is also characterized by
556 a slightly steeper positive correlation between $\delta^{13}\text{C}$ and $\delta^{18}\text{O}$. Both circumstances point to faster
557 hydration/hydroxylation kinetics to be effective during the mineralization of HL compared to its host
558 (Chen et al., 2018). If the pH at which HA precipitates carbonate is lower than the pH of the calcifying
559 fluid in *D. pertusum*, the hydration kinetics would be accelerated as a result (Raddatz et al., 2014;
560 Cohen, 2003; Crenshaw, 1972). Both organisms may derive their carbon from the same source which
561 likely occurs depleted in ^{13}C relative to seawater, possibly due to significant admixture from metabolic
562 CO_2 . This assertion is supported by the fact that HL has constant access to the host's carbon pool.

563 Another mechanism potentially altering the $\delta^{13}\text{C}$ from equilibrium might be the etching mechanism
564 that pumps H^+ -ions in the ambient water around the foraminifera (Toyofuku et al., 2017). The
565 decreasing pH around the foraminifera shifts the carbon speciation towards CO_2 . As CO_2 is depleted in
566 ^{13}C compared to the total inorganic carbon pool, the utilization of CO_2 for calcification would also
567 explain the deviations of the foraminifera's shell $\delta^{13}\text{C}$ from isotopic equilibrium (Toyofuku et al., 2017;
568 McCorkle et al., 1997).

569 **4.6. Implications for paleoceanographic reconstructions**

570 The results presented here have implications for paleoreconstructions in two ways. When using
571 bivalves for paleo reconstructions or geochemical investigations in general, the shells must be carefully
572 examined for potential traces of bioerosion. In case of callus formation, the carbonate formed can
573 have a significantly different composition than the original carbonate mineralogy.

574 Even more critical are the implications for paleoceanographic reconstructions using foraminifera which
575 are regularly analyzed for this purpose. Several foraminifera species are known to live on different host
576 organisms and act as parasites and/or bioeroders (Walker et al., 2017; Dupuy et al., 2010; Freiwald and
577 Schönfeld, 1996). Some of these are also used for isotope and element based paleoenvironmental

578 reconstructions or geochemical investigations in general, such as *Cibicides refulgens* (Mackensen and
579 Nam, 2014; Rathburn and de Deckker, 1997; García-Gallardo et al., 2017), *Hanzawaia concentrica*
580 (Smith and Emiliani, 1968) and *Discanomalia coronata* (Baranwal et al., 2014).

581 As an example, we use a $\delta^{18}\text{O}$ -temperature conversion formula for benthic foraminifera (Marchitto et
582 al., 2014) and our measured $\delta^{18}\text{O}$ ratios to reconstruct a temperature for the Leksa Reef of 7.5 °C using
583 HAO and 7.8 °C using HAW with $\delta^{18}\text{O}_{\text{sw}}$ derived from seawater measurements. *In-situ* measurements
584 of the water temperature in the Leksa Reef by CTD show a mean temperature of 7.8°C (min= 7.1°C,
585 max=8.8°C) (Büscher, 2018). If we however use $\delta^{18}\text{O}$ ratios from HL we would reconstruct a water
586 temperature of 8.8°C and consequently overestimate the water temperature by 1.0 °C

587 If the aforementioned species show similar host specific alterations of their isotopic and elemental
588 composition, paleotemperature reconstructions on the basis of these species could be biased. Given
589 that our results indicate that host specific isotopic and elemental composition changes can be present
590 in the parasitic foraminifera *H. sarcophaga* we draw attention to other parasitic foraminifera that
591 should be investigated for similar host-parasite relations, especially if they are used for geochemical
592 investigations.

593 **4.7. Chemical composition of *H. sarcophaga* compared to other benthic foraminifera**

594 *H. sarcophaga* displays significantly higher Mg/Ca ratios than most other benthic foraminifera species
595 with comparable ecology, that show Mg/Ca ratios between 0.5 and 10 mmol/mol (Lear et al., 2002).
596 Foraminifera that have comparable Mg/Ca ratios to *H. sarcophaga* include *Amphistegina* (23- 77 mmol
597 mol⁻¹ (van Dijk et al., 2019; Raja et al., 2005; Geerken et al., 2018)), *Quinqueloculina* (50 – 135 mmol
598 mol⁻¹ (Gussone et al., 2016; Toyofuku et al., 2000)) and *Pyrgo* (4 – 85 mmol mol⁻¹ (Gussone et al., 2016))
599 but these species are biologically and mineralogically distinct from *H. sarcophaga*. *Quinqueloculina* and
600 *Pyrgo* are porcelaneous, whereas *H. sarcophaga* is hyaline. Furthermore, *H. sarcophaga* is not
601 inhabited by photosymbionts in contrast to *Amphistegina*.

602 The exact processes involved in ion transportation, seawater vacuolization and pH-regulation utilized
603 by *H. sarcophaga* remain to be discovered. High Mg/Ca ratios in *H. sarcophaga* that are similar to
604 inorganic precipitated calcite (Oomori et al., 1987; Mucci and Morse, 1983) may indicate a calcification
605 mechanism without ways of discriminating against elements such as magnesium. These species rely
606 on an increase of the calcification site pH (Erez, 2003; de Nooijer et al., 2009; Toyofuku et al., 2017) to
607 facilitate calcification. The main control on calcite Mg/Ca ratios is then provided by the composition of
608 the calcifying fluid (Raitzsch et al., 2010). The high Mg content would therefore indicate a calcifying
609 space that is more similar to ambient seawater i.e. with no or minor modification via ion channels or
610 pumps (de Nooijer et al., 2014; Bentov and Erez, 2006). Additionally, high Mg/Ca ratios in the calcifying

611 space might be necessary for the stabilization of ACC, a suggested metastable calcite precursor phase
612 in foraminifera and other calcifying organisms (Addadi et al., 2003; Jacob et al., 2011, 2017). High
613 amounts of Mg in the calcite can also cause lattice strain effects, due to the size difference of Mg and
614 Ca ions that causes lattice distortion (Evans et al., 2015; Mucci and Morse, 1983). The lattice distortion
615 can cause an increased incorporation of elements such as Sr and Na (Mucci and Morse, 1983; Evans et
616 al., 2015), a feature that we observe in our samples compared to the species *A. lessonii*, that has slightly
617 lower Mg/Ca ratios than *H. sarcophaga* (35 vs. 45 mmol mol⁻¹) and consequently lower Na/Ca and
618 Sr/Ca ratios (Geerken et al., 2018)

619 **4.8. Biomineralization in the callus region**

620 In order to protect itself from the parasitizing foraminifera, *A. excavata* seals the canal etched through
621 the shell. This is accomplished by rapidly calcifying over the foraminifera boring (Beuck et al., 2008;
622 Cedhagen, 1994). The calcification process produces a callus on the inside of the bivalve shell that is 3-
623 5 mm in diameter and 1-2 mm in height. In the SRZ, evidence can be found for the biomineralization
624 model for bivalves proposed by (Addadi et al., 2006; Checa et al., 2005; Wada and Fujinuki, 1976), i.e.
625 that this process starts with the formation of an organic sheet indicated by the high fluorescence, high
626 S concentration and low Ca concentration of this region, which then acts as a framework during
627 calcification. The following layer is depleted in S and enriched in Ca and therefore represents a higher
628 Ca concentration (Fig. 3 & 4). This sequence is repeated multiple times leading to the formation of the
629 visible callus. As long as the foraminifera does not stop the boring process, the bivalve needs to
630 continually counter the boring process by calcifying in the region of infestation.

631 The callus displays high concentrations of organic material that are not observable in the undisturbed
632 regions. The layers that are characterised by high organic contents appear to be preferentially
633 dissolved (Fig. 3B). In cross sections, organic rich areas make up 50 % of the callus (Fig 1D). It appears
634 unlikely that the high amounts of organic material in the SRZ are solely deposited as a calcification
635 framework, considering the differences between undisturbed shell areas and the SRZ. Therefore, the
636 high amount of deposited organic material probably serves some other purpose, such as an increase
637 of the overall material deposition rate and the provision of an initial sealant from the surrounding
638 water.

639 The Boring organisms pose a threat to the bivalve in multiple ways. It has been shown that *H.*
640 *sarcophaga* penetrated the mantle of *A. excavata* which led to a destruction of the mantle epithelium
641 of the bivalve due to ingestion by *H. sarcophaga* (Cedhagen, 1994). Infested sections showed larger
642 numbers of cell nuclei, indicating higher cell division rates and higher metabolic rates (Cedhagen,
643 1994). The pathway through the bivalve shell furthermore allows pathogens to reach and attack the

644 bivalve and could allow surrounding water to permeate into the extra pallial fluid (EPF) of the bivalve.
645 Even though the EPF in several bivalve species shows trace element concentrations close to seawater
646 (Wada and Fujinuki, 1976; Crenshaw, 1972), the bivalve still has to actively concentrate Ca in the
647 calcifying space to reach concentrations that exceed the solubility product (Wilbur and Saleuddin,
648 1983; Bonucci and Wheeler, 2020). This concentration of Ca is accomplished through active pumping
649 by means of enzymes such as Ca-ATPase (Klein et al., 1996) or through ion channels (Carré et al., 2006).
650 In case of an unsealed calcifying space, the dilution with seawater makes high concentrations of Ca-
651 ions to levels needed for calcification in the extra EPF less likely. A fast-sealing method, by means of
652 organic deposition, is therefore necessary to ensure that the bivalve's calcification capability is not
653 compromised.

654 Geochemically, the SRZ shows the largest differences to the undisturbed aragonite in Mg/Ca and Sr/Ca
655 ratios (Fig 2 & 3). Mg/Ca ratios are five times higher in the SRZ than in undisturbed aragonite.
656 Magnesium is thought to be enriched in organic matrices secreted by the bivalve compared to the shell
657 CaCO₃ (Schöne et al., 2010). The distribution of magnesium in the SRZ, especially its enrichment in
658 fluorescent layers rich in sulfur (Fig. 1,3 and 4), makes an enrichment of Mg due to high organic
659 concentrations likely. Beside an enrichment of Mg in the secreted organic matter, peptides similar to
660 that found at the site of calcification in bivalves (Moradian-Oldak et al., 1990) can increase the Mg
661 concentration in precipitated calcite by reducing the dehydration enthalpy (Stephenson et al., 2008).
662 These peptides are also regularly found in molluscs (Marin et al., 2007; Falini et al., 1996; Halloran and
663 Donachy, 1995; Zhang and Zhang, 2006). As these peptides do furthermore increase the growth rate
664 by 25 % to 50 % (Stephenson et al., 2008), due to the need of fast calcification (Beuck et al., 2008), it
665 may suggest that a high concentration of peptides in the SRZ is likely. Higher growth rates can
666 additionally lead to an increase of crystal impurities which could alter other elements besides Mg
667 (Lorens, 1981).

668 In contrast to Mg, Sr was not found to be enriched in organic matter compared to shell CaCO₃ (Takesue
669 et al., 2008), and therefore the presence of organics cannot explain the observed high Sr/Ca of the
670 aragonite in the SRZ. Yet, there is evidence for the influence of peptides on the incorporation of other
671 elements such as Sr (Stephenson et al., 2008). Sr incorporation in the aragonitic bivalves is considered
672 to be controlled in-part by growth rate effects (Lorrain et al., 2005; Füllenbach et al., 2017; Takesue et
673 al., 2008; Carré et al., 2006). A calcification rate control on Sr incorporation is also supported from
674 abiogenic calcite (Gabitov et al., 2014) but not from abiogenic aragonite (Gabitov et al., 2006).
675 Accordingly, this growth rate effect is probably of biologic nature in aragonite precipitates.

676 Sr likely arrives into the calcifying space via similar pathways as Ca, as was shown by the effects of
677 calcium channel blockers in corals (Ferrier-Pagès et al., 2002). However, Ca-ATPase has a higher affinity

678 for Ca than Sr (Yu and Inesi, 1995). Therefore, a higher Ca-ATPase activity, as a result of increased
679 growth rates, should lead to decreasing Sr/Ca ratios in the precipitates, which was shown in corals
680 (Ferrier-Pagès et al., 2002; de Villiers et al., 1995). As we expect high growth rates in the SRZ, Ca
681 channels that also transport Sr cannot explain the observed Sr distribution in this zone. Alternatively,
682 the organism's metabolic rate has been suggested to control Sr/Ca in bivalves through metabolic
683 pumping (Klein et al., 1996). High metabolic activity was observed in *A. excavata* infested by *H.*
684 *sarcophaga*, indicated by a high concentration of cell-nuclei (Cedhagen, 1994). The model of Klein et
685 al. (1996) would predict lower Sr/Ca ratios in these areas, thus a mechanism other than metabolic
686 pumping must control the high Sr/Ca ratios in the SRZ.

687 Füllenbach et al. (2015) proposed that in slow growing areas of bivalves, the organisms exert less
688 biological control over element incorporation, leading to elevated Sr/Ca ratios. While this hypothesis
689 does not fit to our observation of elevated Sr/Ca ratios in a potentially fast-growing shell area, a similar
690 hypothesis was suggested concerning Mg/Ca in *Mytilus edulis* (Lorens and Bender, 1980). The authors
691 found strongly elevated Mg/Ca ratios in shells sections that were precipitated after handling the
692 specimens for size measurements and attributed this effect to stress (Lorens and Bender, 1980). The
693 boring of *H. sarcophaga* is very likely to be a stress factor on *A. excavata*. An influence of such stress
694 related effects on Mg/Ca and potentially Sr/Ca (Fig. 4) are, therefore, possible. The high Mg-
695 concentrations in the EPF due to a potential breakdown of Mg-regulating mechanisms however, would
696 inhibit the organism from calcification due to the inhibiting effects of Mg on crystal nucleation and
697 growth (Pytkowicz, 1965; Lorens and Bender, 1980). *A. excavata* might circumvent this by releasing
698 additional sulphate bearing organic molecules that provide additional nucleation sites and higher Ca-
699 concentrations at the nucleation sites (Lorens and Bender, 1980), which might potentially be the cause
700 of the observed increased S/Ca ratios in the SRZ (Fig. 4).

701

702 **5. Conclusion**

703 Our results demonstrate that the elemental and isotopic composition of the parasitic foraminifera *H.*
704 *sarcophaga* varies depending on the host organisms that the foraminifera settle on. *H. sarcophaga*
705 that lived on the coral *D. pertusum* shows significantly higher Sr/Ca ratios than those that lived on the
706 bivalve *A. excavata*. Combining these data with a simple mixing model, we propose that this could
707 point towards a biomineralization pathway that is influenced by uptake of carbonate material derived
708 from the host. The dissolution of the host shell could serve to satisfy the foraminifera's demand for
709 calcium and DIC.

710 We also observe significant differences between *H. sarcophaga* specimens that grew on *A. excavata*
711 that can be correlated to the success of the penetration progress. Foraminifera that fully penetrated
712 the bivalve's shell, recognizable by the hosts callus formation, display significantly lower Mn/Ca ratios
713 than foraminifera that did not completely penetrate the shell. This could be an effect of a suspension
714 feeding period of the foraminifera or grazing of Mn-rich material of the periostracum until it
715 penetrated the bivalve's shell when switching to a parasitic mode of feeding. Other possibilities include
716 differences in the growth rate caused by changes of the nutrient availability or Rayleigh fractionation.

717 The oxygen and carbon isotopic composition of *H. sarcophaga* also appears to be influenced by the
718 type of host organism that it infests. Again, this might be an effect of a direct uptake of the host's
719 organic material and/or CaCO₃. Other effects such as different pH regimes in the host organisms and
720 varying equilibration may also play a role. Different extents of the calcification site carbonate system
721 equilibration between *H. sarcophaga* that infested *D. pertusum* (HL) and *H. sarcophaga* that infested
722 *A. excavata* (HA) could also explain the missing signs of kinetic fractionation in HL compared to HA.

723 As the elemental and isotopic composition of some parasitic foraminifera is used for
724 paleoceanographic reconstructions, our results indicate that such studies should only be performed
725 when the host organism is known.

726 **Author contribution**

727 **NS:** Investigation, Conceptualization, Data curation, formal analysis, Investigation, Visualization,
728 Writing (Original Draft)

729 **DE:** Methodology, Formal Analysis, Writing (Review & Editing)

730 **MW:** Resources, Writing (Review & Editing)

731 **JVB:** Resources, Writing (Review & Editing)

732 **JF:** Investigation, Resources, Writing (Review & Editing)

733 **AF:** Resources, Writing (Review & Editing)

734 **SH:** Investigation, Writing (Review & Editing)

735 **HM:** Investigation, Resources, Writing (Review & Editing)

736 **SV:** Supervision, Resources, Writing (Review & Editing)

737 **JR:** Funding Acquisition, Investigation, Project administration, Supervision, Resources, Writing (Review
738 & Editing)

739 **Acknowledgments**

740 We are grateful to all cruise captains, crew members and cruise participants of research cruises
741 POS473 and POS525. We are also grateful for the help of Celestine Beyer and Luciano Zolezzi, who
742 aided with the EPMA measurements. We also want to thank Lennart de Nooijer and Inge van Dijk,
743 whose detailed comments substantially improved our manuscript. This work was funded by the
744 Deutsche Forschungsgemeinschaft, RA 2156-5/1 to JR. This is FIERCE contribution No. 75

745 **Supplements**

746 [1] Pictures of Meigen test

747 [2] Measurement data

748 [3] RAW and TIFF pictures of Fig.1

749 **Competing Interests**

750 The authors declare that they have no conflict of interest.

751 **References**

752 Addadi, L., Raz, S., and Weiner, S.: Taking Advantage of Disorder: Amorphous Calcium Carbonate and
753 Its Roles in Biomineralization, *Advanced Materials*, 15, 959–970,
754 <https://doi.org/10.1002/adma.200300381>, 2003.

755 Addadi, L., Joester, D., Nudelman, F., and Weiner, S.: Mollusk Shell Formation: A Source of New
756 Concepts for Understanding Biomineralization Processes, *Chemistry - A European Journal*, 12, 980–
757 987, <https://doi.org/10.1002/chem.200500980>, 2006.

758 Addamo, A. M., Vertino, A., Stolarski, J., García-Jiménez, R., Taviani, M., and Machordom, A.: Merging
759 scleractinian genera: The overwhelming genetic similarity between solitary *Desmophyllum* and
760 colonial *Lophelia*, *BMC Evolutionary Biology*, 16, <https://doi.org/10.1186/s12862-016-0654-8>, 2016.

761 Adkins, J. F., Boyle, E. A., Curry, W. B., and Lutringer, A.: Stable isotopes in deep-sea corals and a new
762 mechanism for “vital effects,” *Geochimica et Cosmochimica Acta*, 67, 1129–1143,
763 [https://doi.org/10.1016/S0016-7037\(02\)01203-6](https://doi.org/10.1016/S0016-7037(02)01203-6), 2003.

764 Alexander, S. P. and Delaca, T. E.: Feeding adaptations of the foraminiferan *Cibicides refulgens* living
765 epizoically and parasitically on the Antarctic scallop *Adamussium colbecki*, *Biological Bulletin*, 173,
766 136–159, <https://doi.org/10.2307/1541868>, 1987.

767 Allen, J. A.: Manganese deposition on the shells of living molluscs, *Nature*, 185, 336–337,
768 <https://doi.org/10.1038/185336b0>, 1960.

769 Bajnai, D., Fiebig, J., Tomašových, A., Milner Garcia, S., Rollion-Bard, C., Raddatz, J., Löffler, N., Primo-
770 Ramos, C., and Brand, U.: Assessing kinetic fractionation in brachiopod calcite using clumped
771 isotopes, *Scientific Reports*, 8, 533, <https://doi.org/10.1038/s41598-017-17353-7>, 2018.

772 Baranwal, S., Sauer, S., Knies, J., Chand, S., Jensen, H., and Klug, M.: Benthic foraminifera as tools in
773 interpretation of subsurface hydrocarbon fluid flow at Veslemøy High and Hola-Vesterålen areas of
774 the Barents Sea, *Geophysical Research Abstracts*, 2014-1843 pp., 2014.

775 Bentov, S. and Erez, J.: Impact of biomineralization processes on the Mg content of foraminiferal
776 shells: A biological perspective, *Geochemistry, Geophysics, Geosystems*, 7,
777 <https://doi.org/10.1029/2005GC001015>, 2006.

778 Beuck, L., López Correa, M., and Freiwald, A.: Biogeographical distribution of Hyrrokkin (*Rosalinidae*,
779 *Foraminifera*) and its host-specific morphological and textural trace variability, *Current*
780 *Developments in Bioerosion*, 329–360, <https://doi.org/10.1007/978-3-540-77598-0-17>, 2008.

781 Bonucci, E. and Wheeler, A. P.: Mechanisms of Molluscan Shell Formation, in: *Calcification in*
782 *Biological Systems*, Plenum Press, 179–216, <https://doi.org/10.1201/9781003068396-10>, 2020.

783 Büscher, J.: Cold-water coral habitat characterisation and in situ physiological state analyses of four
784 spatially distinct reefs in North- and mid-Norway-Cruise Report RV POSEIDON 525 [POS525],
785 GEOMAR, Kiel, Germany, https://doi.org/10.3289/CR_POS525, 2018.

786 Calvert, S. E. and Pedersen, T. F.: Geochemistry of Recent oxic and anoxic marine sediments:
787 Implications for the geological record, *Marine Geology*, [https://doi.org/10.1016/0025-](https://doi.org/10.1016/0025-3227(93)90150-T)
788 [3227\(93\)90150-T](https://doi.org/10.1016/0025-3227(93)90150-T), 1993.

789 Calvert, S. E. and Pedersen, T. F.: Sedimentary geochemistry of manganese: Implications for the
790 environment of formation of manganese black shales, *Economic Geology*,
791 <https://doi.org/10.2113/gsecongeo.91.1.36>, 1996.

792 Carré, M., Bentaleb, I., Bruguier, O., Ordinola, E., Barrett, N. T., and Fontugne, M.: Calcification rate
793 influence on trace element concentrations in aragonitic bivalve shells: Evidences and mechanisms,
794 *Geochimica et Cosmochimica Acta*, 70, 4906–4920, <https://doi.org/10.1016/j.gca.2006.07.019>, 2006.

795 Cedhagen, T.: Taxonomy and biology of hyrrokkin *sarcophaga* gen. Et Sp. N., a parasitic foraminiferan
796 (*rosalinidae*), *Sarsia*, 79, 65–82, <https://doi.org/10.1080/00364827.1994.10413549>, 1994.

797 Checa, A. G., Rodríguez-Navarro, A. B., and Esteban-Delgado, F. J.: The nature and formation of
798 calcitic columnar prismatic shell layers in pteriomorphian bivalves, *Biomaterials*, 26, 6404–6414,
799 <https://doi.org/10.1016/j.biomaterials.2005.04.016>, 2005.

800 Chen, S., Gagnon, A. C., and Adkins, J. F.: Carbonic anhydrase, coral calcification and a new model of
801 stable isotope vital effects, *Geochimica et Cosmochimica Acta*, 236, 179–197,
802 <https://doi.org/10.1016/j.gca.2018.02.032>, 2018.

803 Cheng, Y. R. and Dai, C. F.: A bioeroding foraminifer, *Hyrrokkin sarcophaga*, on deepwater corals from
804 the South China Sea, *Coral Reefs*, 35, 901, <https://doi.org/10.1007/s00338-016-1447-7>, 2016.

805 Cohen, A. L.: Geochemical Perspectives on Coral Mineralization, *Reviews in Mineralogy and*
806 *Geochemistry*, 54, 151–187, <https://doi.org/10.2113/0540151>, 2003.

807 Crenshaw, M. A.: The inorganic composition of molluscan extrapallial fluid, *The Biological Bulletin*,
808 143, 506–512, <https://doi.org/10.2307/1540180>, 1972.

809 Culver, S. J.: Early Cambrian foraminifera from West Africa, *Science*, 254, 689–691,
810 <https://doi.org/10.1126/science.254.5032.689>, 1991.

811 van Dijk, I., Mouret, A., Cotte, M., le Houedec, S., Oron, S., Reichart, G. J., Reyes-Herrera, J., Filipsson,
812 H. L., and Barras, C.: Chemical Heterogeneity of Mg, Mn, Na, S, and Sr in Benthic Foraminiferal
813 Calcite, *Frontiers in Earth Science*, 7, 281, <https://doi.org/10.3389/feart.2019.00281>, 2019.

814 van Dijk, I., de Nooijer, L. J., Barras, C., and Reichart, G. J.: Mn Incorporation in Large Benthic
815 Foraminifera: Differences Between Species and the Impact of pCO₂, *Frontiers in Earth Science*,
816 <https://doi.org/10.3389/feart.2020.567701>, 2020.

817 Dupuy, C., Rossignol, L., Geslin, E., and Pascal, P. Y.: Predation of mudflat meio-macrofaunal
818 metazoans by a calcareous foraminifer, *Ammonia tepida* (Cushman, 1926), *Journal of Foraminiferal*
819 *Research*, 40, 305–312, <https://doi.org/10.2113/gsjfr.40.4.305>, 2010.

820 Elderfield, H.: A biomineralization model for the incorporation of trace elements into foraminiferal
821 calcium carbonate, *Earth and Planetary Science Letters*, 142, 409–423, [https://doi.org/10.1016/0012-](https://doi.org/10.1016/0012-821X(96)00105-7)
822 [821X\(96\)00105-7](https://doi.org/10.1016/0012-821X(96)00105-7), 1996.

823 Erez, J.: The Source of Ions for Biomineralization in Foraminifera and Their Implications for
824 Paleooceanographic Proxies, *Reviews in Mineralogy and Geochemistry*, 54, 115–149,
825 <https://doi.org/10.2113/0540115>, 2003.

826 Evans, D., Erez, J., Oron, S., and Müller, W.: Mg/Ca-temperature and seawater-test chemistry
827 relationships in the shallow-dwelling large benthic foraminifera *Operculina ammonoides*, *Geochimica*
828 *et Cosmochimica Acta*, 148, 325–342, <https://doi.org/10.1016/j.gca.2014.09.039>, 2015.

829 Evans, D., Müller, W., and Erez, J.: Assessing foraminifera biomineralisation models through trace
830 element data of cultures under variable seawater chemistry, *Geochimica et Cosmochimica Acta*, 236,
831 198–217, <https://doi.org/10.1016/j.gca.2018.02.048>, 2018.

832 Falini, G., Albeck, S., Weiner, S., and Addadi, L.: Control of Aragonite or Calcite Polymorphism by
833 Mollusk Shell Macromolecules, *Science*, 271, 67–69, <https://doi.org/10.1126/science.271.5245.67>,
834 1996.

835 Ferrier-Pagès, C., Boisson, F., Allemand, D., and Tambutté, E.: Kinetics of strontium uptake in the
836 scleractinian coral *Stylophora pistillata*, *Marine Ecology Progress Series*, 245, 93–100,
837 <https://doi.org/10.3354/meps245093>, 2002.

838 Form, A. U., Büscher, J. v., Hissmann, K., Flögel, S., Wisshak, M., Rüggeberg, A., Bannister, R., Kutti, T.,
839 Stapp, L., Bennecke, S., Küter, M., Nachtigall, K., Schauer, J., and Fenske, M.: RV POSEIDON Cruise
840 Report POS473 LORELEI II: LOfelia REef Lander Expedition and Investigation II, Tromsø – Bergen –
841 Esbjerg, 15.08. – 31.08. – 04.09.2014., 25 pp., https://doi.org/10.3289/CR_POS_473, 2015.

842 Freiwald, A. and Schönfeld, J.: Substrate pitting and boring pattern of *Hyrrokkin sarcophaga*
843 *Cedhagen*, 1994 (Foraminifera) in a modern deep-water coral reef mound, *Marine*
844 *Micropaleontology*, 28, 199–207, 1996.

845 Füger, A., Konrad, F., Leis, A., Dietzel, M., and Mavromatis, V.: Effect of growth rate and pH on
846 lithium incorporation in calcite, *Geochimica et Cosmochimica Acta*, 248, 14–24,
847 <https://doi.org/10.1016/j.gca.2018.12.040>, 2019.

848 Füllenbach, C. S., Schöne, B. R., Shirai, K., Takahata, N., Ishida, A., and Sano, Y.: Minute co-variations
849 of Sr/Ca ratios and microstructures in the aragonitic shell of *Cerastoderma edule* (Bivalvia) – Are
850 geochemical variations at the ultra-scale masking potential environmental signals?, *Geochimica et*
851 *Cosmochimica Acta*, 205, 256–271, <https://doi.org/10.1016/j.gca.2017.02.019>, 2017.

852 Gabitov, R. I., Cohen, A. L., Gaetani, G. A., Holcomb, M., and Watson, E. B.: The impact of crystal
853 growth rate on element ratios in aragonite: An experimental approach to understanding vital effects,
854 *Geochimica et Cosmochimica Acta*, 70, A187, <https://doi.org/10.1016/j.gca.2006.06.377>, 2006.

855 Gabitov, R. I., Sadekov, A., and Leinweber, A.: Crystal growth rate effect on Mg/Ca and Sr/Ca
856 partitioning between calcite and fluid: An in situ approach, *Chemical Geology*, 367, 70–82,
857 <https://doi.org/10.1016/j.chemgeo.2013.12.019>, 2014.

858 García-Gallardo, Á., Grunert, P., Voelker, A. H. L., Mendes, I., and Piller, W. E.: Re-evaluation of the
859 “elevated epifauna” as indicator of Mediterranean Outflow Water in the Gulf of Cadiz using stable
860 isotopes ($\delta^{13}\text{C}$, $\delta^{18}\text{O}$), *Global and Planetary Change*, 155, 78–97,
861 <https://doi.org/10.1016/j.gloplacha.2017.06.005>, 2017.

862 Geerken, E., Jan De Nooijer, L., van Dijk, I., and Reichart, G. J.: Impact of salinity on element
863 incorporation in two benthic foraminiferal species with contrasting magnesium contents,
864 *Biogeosciences*, 15, 2205–2218, <https://doi.org/10.5194/bg-15-2205-2018>, 2018.

865 GEOMAR Helmholtz-Zentrum für Ozeanforschung: Research Vessel POSEIDON, *Journal of large-scale*
866 *research facilities JLSRF*, 1, 60–63, <https://doi.org/10.17815/jlsrf-1-62>, 2015.

867 GEOMAR Helmholtz-Zentrum für Ozeanforschung: Manned submersible „JAGO“, *Journal of large-*
868 *scale research facilities JLSRF*, 3, 1–12, <https://doi.org/10.17815/jlsrf-3-157>, 2017.

869 Goldstein, J. I., Newbury, D. E., Michael, J. R., Ritchie, N. W. M., Scott, J. H. J., and Joy, D. C.: *Scanning*
870 *Electron Microscopy and X-Ray Microanalysis*, Springer New York, New York, NY,
871 <https://doi.org/10.1007/978-1-4939-6676-9>, 2018.

872 Goldstein, S. T.: Foraminifera: A biological overview, in: *Modern Foraminifera*,
873 https://doi.org/10.1007/0-306-48104-9_3, 1999.

874 Gray, W. R. and Evans, D.: Nonthermal Influences on Mg/Ca in Planktonic Foraminifera: A Review of
875 Culture Studies and Application to the Last Glacial Maximum, *Paleoceanography and*
876 *Paleoclimatology*, 34, 306–315, <https://doi.org/10.1029/2018PA003517>, 2019.

877 Greaves, M., Barker, S., Daunt, C., and Elderfield, H.: Accuracy, standardization, and interlaboratory
878 calibration standards for foraminiferal Mg/Ca thermometry, *Geochemistry, Geophysics, Geosystems*,
879 6, 2–13, <https://doi.org/10.1029/2004GC000790>, 2005.

880 Greaves, M., Caillon, N., Rebaubier, H., Bartoli, G., Bohaty, S., Cacho, I., Clarke, L., Cooper, M., Daunt,
881 C., Delaney, M., DeMenocal, P., Dutton, A., Eggins, S., Elderfield, H., Garbe-Schoenberg, D., Goddard,
882 E., Green, D., Groeneveld, J., Hastings, D., Hathorne, E., Kimoto, K., Klinkhammer, G., Labeyrie, L., Lea,
883 D. W., Marchitto, T., Martínez-Botí, M. A., Mortyn, P. G., Ni, Y., Nuernberg, D., Paradis, G., Quinn, T.,
884 Rosenthal, Y., Russel, A., Sagawa, T., Sosdian, S., Stott, L., Tachikawa, K., Tappa, E., Thunell, R., and
885 Wilson, P. A.: Interlaboratory comparison study of calibration standards for foraminiferal Mg/Ca

886 thermometry, *Geochemistry, Geophysics, Geosystems*, 9, 1–27,
887 <https://doi.org/10.1029/2008GC001974>, 2008.

888 Groeneveld, J. and Filipsson, H. L.: Mg/Ca and Mn/Ca ratios in benthic foraminifera: the potential to
889 reconstruct past variations in temperature and hypoxia in shelf regions, *Biogeosciences*, 10, 5125–
890 5138, <https://doi.org/10.5194/bg-10-5125-2013>, 2013.

891 Gussone, N., Filipsson, H. L., and Kuhnert, H.: Mg/Ca, Sr/Ca and Ca isotope ratios in benthonic
892 foraminifers related to test structure, mineralogy and environmental controls, *Geochimica et*
893 *Cosmochimica Acta*, 173, 142–159, <https://doi.org/10.1016/j.gca.2015.10.018>, 2016.

894 Halloran, B. A. and Donachy, J. E.: Characterization of organic matrix macromolecules from the shells
895 of the antarctic scallop, *Adamussium colbecki*, *Comparative Biochemistry and Physiology -- Part B:*
896 *Biochemistry and*, 111, 221–231, [https://doi.org/10.1016/0305-0491\(94\)00245-P](https://doi.org/10.1016/0305-0491(94)00245-P), 1995.

897 Hancock, L. G., Walker, S. E., Pérez-Huerta, A., and Bowser, S. S.: Population Dynamics and Parasite
898 Load of a Foraminifer on Its Antarctic Scallop Host with Their Carbonate Biomass Contributions, *PLOS*
899 *ONE*, 10, e0132534, <https://doi.org/10.1371/journal.pone.0132534>, 2015.

900 Holland, K., Eggins, S. M., Hönisch, B., Haynes, L. L., and Branson, O.: Calcification rate and shell
901 chemistry response of the planktic foraminifer *Orbulina universa* to changes in microenvironment
902 seawater carbonate chemistry, *Earth and Planetary Science Letters*, 464, 124–134,
903 <https://doi.org/10.1016/j.epsl.2017.02.018>, 2017.

904 Hönisch, B., Allen, K. A., Russell, A. D., Eggins, S. M., Bijma, J., Spero, H. J., Lea, D. W., and Yu, J.:
905 Planktic foraminifers as recorders of seawater Ba/Ca, *Marine Micropaleontology*, 79, 52–57,
906 <https://doi.org/10.1016/j.marmicro.2011.01.003>, 2011.

907 Horton, T., Kroh, A., Ahyong, S., Bailly, N., Boyko, C. B., Brandão, S. N., Gofas, S., Hooper, J. N. A.,
908 Hernandez, F., Holovachov, O., Mees, J., Molodtsova, T. N., Paulay, G., Decock, W., Dekeyzer, S.,
909 Poffyn, G., Vandepitte, L., Vanhoorne, B., Adlard, R., Agatha, S., Ahn, K. J., Akkari, N., Alvarez, B.,
910 Anderberg, A., Anderson, G., Angel, M. v, Antic, D., Arango, C., Artois, T., Atkinson, S., Auffenberg, K.,
911 Baldwin, B. G., Bank, R., Barber, A., Barbosa, J. P., Bartsch, I., Bellan-Santini, D., Bergh, N., Bernot, J.,
912 Berta, A., Bezerra, T. N., Bieler, R., Blanco, S., Blasco-Costa, I., Blazewicz, M., Bock, P., Bonifacino de
913 León, M., Böttger-Schnack, R., Bouchet, P., Boury-Esnault, N., Boxshall, G., Bray, R., Bruce, N. L.,
914 Cairns, S., Calvo Casas, J., Carballo, J. L., Cárdenas, P., Carstens, E., Chan, B. K., Chan, T. Y., Cheng, L.,
915 Christenhusz, M., Churchill, M., Coleman, C. O., Collins, A. G., Collins, G. E., Corbari, L., Cordeiro, R.,
916 Cornils, A., Coste, M., Costello, M. J., Crandall, K. A., Cremonte, F., Cribb, T., Cutmore, S., Dahdouh-
917 Guebas, F., Daly, M., Daneliya, M., Dauvin, J. C., Davie, P., de Broyer, C., de Grave, S., de Mazancourt,

918 V., de Voogd, N. J., Decker, P., Defaye, D., d'Hondt, J. L., Dippenaar, S., Dohrmann, M., Dolan, J.,
919 Domning, D., Downey, R., Ector, L., Eisendle-Flöckner, U., Eitel, M., Encarnaç o, S. C. d., Enghoff, H.,
920 Epler, J., Ewers-Saucedo, C., et al.: World Register of Marine Species (WoRMS),
921 <http://www.marinespecies.org>, 2021.

922 Immenhauser, A., Sch ne, B. R., Hoffmann, R., and Niedermayr, A.: Mollusc and brachiopod skeletal
923 hard parts: Intricate archives of their marine environment, *Sedimentology*, 63, 1–59,
924 <https://doi.org/10.1111/sed.12231>, 2016.

925 Jacob, D. E., Wirth, R., Soldati, A. L., Wehrmeister, U., and Schreiber, A.: Amorphous calcium
926 carbonate in the shells of adult Unionoida, *Journal of Structural Biology*, 173, 241–249,
927 <https://doi.org/10.1016/j.jsb.2010.09.011>, 2011.

928 Jacob, D. E., Wirth, R., Agbaje, O. B. A., Branson, O., and Eggins, S. M.: Planktic foraminifera form
929 their shells via metastable carbonate phases, *Nature Communications*, 8, 1–8,
930 <https://doi.org/10.1038/s41467-017-00955-0>, 2017.

931 Jacobson, P.: Physical Oceanography of the Trondheimsfjord, *Geophysical & Astrophysical Fluid
932 Dynamics*, 26, 3–26, <https://doi.org/10.1080/03091928308221761>, 1983.

933 Jochum, K. P., Nohl, U., Herwig, K., Lammel, E., Stoll, B., and Hofmann, A. W.: GeoReM: A New
934 Geochemical Database for Reference Materials and Isotopic Standards, *Geostandards and
935 Geoanalytical Research*, 29, 333–338, <https://doi.org/10.1111/j.1751-908X.2005.tb00904.x>, 2005.

936 Kato, K., Wada, H., and Fujioka, K.: The application of chemical staining to separate calcite and
937 aragonite minerals for micro-scale isotopic analyses, *Geochemical Journal*, 37, 291–297,
938 <https://doi.org/10.2343/geochemj.37.291>, 2003.

939 Klein, R. T., Lohmann, K. C., and Thayer, C. W.: Sr/Ca and $^{13}\text{C}/^{12}\text{C}$ ratios in skeletal calcite of *Mytilus
940 trossulus*: Covariation with metabolic rate, salinity, and carbon isotopic composition of seawater,
941 *Geochimica et Cosmochimica Acta*, [https://doi.org/10.1016/S0016-7037\(96\)00232-3](https://doi.org/10.1016/S0016-7037(96)00232-3), 1996.

942 Koho, K. A., de Nooijer, L. J., and Reichart, G. J.: Combining benthic foraminiferal ecology and shell
943 Mn/Ca to deconvolve past bottom water oxygenation and paleoproductivity, *Geochimica et
944 Cosmochimica Acta*, 165, 294–306, <https://doi.org/10.1016/j.gca.2015.06.003>, 2015.

945 Lantz, B.: The impact of sample non-normality on ANOVA and alternative methods, *British Journal of
946 Mathematical and Statistical Psychology*, 66, 224–244, [https://doi.org/10.1111/j.2044-
947 8317.2012.02047.x](https://doi.org/10.1111/j.2044-8317.2012.02047.x), 2013.

948 Lear, C. H. and Rosenthal, Y.: Benthic foraminiferal Li/Ca: Insights into Cenozoic seawater carbonate
949 saturation state, *Geology*, 34, 985, <https://doi.org/10.1130/G22792A.1>, 2006.

950 Lear, C. H., Rosenthal, Y., and Slowey, N.: Benthic foraminiferal Mg/Ca-paleothermometry: A revised
951 core-top calibration, *Geochimica et Cosmochimica Acta*, 66, 3375–3387,
952 [https://doi.org/10.1016/S0016-7037\(02\)00941-9](https://doi.org/10.1016/S0016-7037(02)00941-9), 2002.

953 Lorens, R. B.: Sr, Cd, Mn and Co distribution coefficients in calcite as a function of calcite precipitation
954 rate, *Geochimica et Cosmochimica Acta*, 45, 553–561, [https://doi.org/10.1016/0016-7037\(81\)90188-](https://doi.org/10.1016/0016-7037(81)90188-5)
955 5, 1981.

956 Lorens, R. B. and Bender, M. L.: The impact of solution chemistry on *Mytilus edulis* calcite and
957 aragonite, *Geochimica et Cosmochimica Acta*, 44, 1265–1278, [https://doi.org/10.1016/0016-](https://doi.org/10.1016/0016-7037(80)90087-3)
958 7037(80)90087-3, 1980.

959 Lorrain, A., Gillikin, D. P., Paulet, Y. M., Chauvaud, L., le Mercier, A., Navez, J., and André, L.: Strong
960 kinetic effects on Sr/Ca ratios in the calcitic bivalve *Pecten maximus*, *Geology*, 33, 965–968,
961 <https://doi.org/10.1130/G22048.1>, 2005.

962 Mackensen, A. and Nam, S. il: Taxon-specific epibenthic foraminiferal $\delta^{18}\text{O}$ in the Arctic Ocean:
963 Relationship to water masses, deep circulation, and brine release, *Marine Micropaleontology*, 113,
964 34–43, <https://doi.org/10.1016/j.marmicro.2014.09.002>, 2014.

965 Marchitto, T. M., Curry, W. B., Lynch-Stieglitz, J., Bryan, S. P., Cobb, K. M., and Lund, D. C.: Improved
966 oxygen isotope temperature calibrations for cosmopolitan benthic foraminifera, *Geochimica et*
967 *Cosmochimica Acta*, 130, 1–11, <https://doi.org/10.1016/j.gca.2013.12.034>, 2014.

968 Marin, F., Luquet, G., Marie, B., and Medakovic, D.: Molluscan Shell Proteins: Primary Structure,
969 Origin, and Evolution, *Current Topics in Developmental Biology*, 80, 209–276,
970 [https://doi.org/10.1016/S0070-2153\(07\)80006-8](https://doi.org/10.1016/S0070-2153(07)80006-8), 2007.

971 McConnaughey, T. A.: Sub-equilibrium oxygen-18 and carbon-13 levels in biological carbonates:
972 Carbonate and kinetic models, *Coral Reefs*, 22, 316–327, [https://doi.org/10.1007/s00338-003-0325-](https://doi.org/10.1007/s00338-003-0325-2)
973 2, 2003.

974 McCorkle, D. C., Corliss, B. H., and Farnham, C. A.: Vertical distributions and stable isotopic
975 compositions of live (stained) benthic foraminifera from the North Carolina and California continental
976 margins, *Deep-Sea Research Part I: Oceanographic Research Papers*, 44, 983–1024,
977 [https://doi.org/10.1016/S0967-0637\(97\)00004-6](https://doi.org/10.1016/S0967-0637(97)00004-6), 1997.

978 McCulloch, M., Falter, J., Trotter, J., and Montagna, P.: Coral resilience to ocean acidification and
979 global warming through pH up-regulation, *Nature Climate Change*, 2, 623–627,
980 <https://doi.org/10.1038/nclimate1473>, 2012.

981 Mienis, F., de Stigter, H. C., White, M., Duineveld, G., de Haas, H., and van Weering, T. C. E.:
982 Hydrodynamic controls on cold-water coral growth and carbonate-mound development at the SW
983 and SE Rockall Trough Margin, NE Atlantic Ocean, *Deep-Sea Research Part I: Oceanographic Research*
984 *Papers*, 54, 1655–1674, <https://doi.org/10.1016/j.dsr.2007.05.013>, 2007.

985 Milzer, G., Giraudeau, J., Faust, J., Knies, J., Eynaud, F., and Rühlemann, C.: Spatial distribution of
986 benthic foraminiferal stable isotopes and dinocyst assemblages in surface sediments of the
987 Trondheimsfjord, central Norway, *Biogeosciences*, 10, 4433–4448, [https://doi.org/10.5194/bg-10-](https://doi.org/10.5194/bg-10-4433-2013)
988 [4433-2013](https://doi.org/10.5194/bg-10-4433-2013), 2013.

989 Moradian-Oldak, J., Addadi, L., Weiner, S., and Berman, A.: Tuning of Crystal Nucleation and Growth
990 by Proteins: Molecular Interactions at Solid-Liquid Interfaces in Biomineralization, *Croatica Chemica*
991 *Acta*, 63, 539–544, 1990.

992 Mucci, A.: Manganese uptake during calcite precipitation from seawater: Conditions leading to the
993 formation of a pseudokutnahorite, *Geochimica et Cosmochimica Acta*, 52, 1859–1868,
994 [https://doi.org/10.1016/0016-7037\(88\)90009-9](https://doi.org/10.1016/0016-7037(88)90009-9), 1988.

995 Mucci, A. and Morse, J. W.: The incorporation of Mg²⁺ and Sr²⁺ into calcite overgrowths: influences
996 of growth rate and solution composition, *Geochimica et Cosmochimica Acta*, 47, 217–233, 1983.

997 Nakahara, H.: Nacre Formation in Bivalve and Gastropod Molluscs, in: *Mechanisms and Phylogeny of*
998 *Mineralization in Biological Systems*, Springer Japan, Tokyo, 343–350, [https://doi.org/10.1007/978-4-](https://doi.org/10.1007/978-4-431-68132-8_55)
999 [431-68132-8_55](https://doi.org/10.1007/978-4-431-68132-8_55), 1991.

1000 Nehrke, G., Keul, N., Langer, G., de Nooijer, L. J., Bijma, J., and Meibom, A.: A new model for
1001 biomineralization and trace-element signatures of Foraminifera tests, *Biogeosciences*,
1002 <https://doi.org/10.5194/bg-10-6759-2013>, 2013.

1003 de Nooijer, L. J., Toyofuku, T., and Kitazato, H.: Foraminifera promote calcification by elevating their
1004 intracellular pH, *Proceedings of the National Academy of Sciences of the United States of America*,
1005 106, 15374–15378, <https://doi.org/10.1073/pnas.0904306106>, 2009.

1006 de Nooijer, L. J., Spero, H. J., Erez, J., Bijma, J., and Reichart, G. J.: Biomineralization in perforate
1007 foraminifera, *Earth-Science Reviews*, 135, 48–58, <https://doi.org/10.1016/j.earscirev.2014.03.013>,
1008 2014.

1009 Oomori, T., Kaneshima, H., Maezato, Y., and Kitano, Y.: Distribution Coefficient of Mg²⁺ ions between
1010 calcite and solution at 10-50°C, *Marine Chemistry*, 20, 327–336, [https://doi.org/10.1016/B978-](https://doi.org/10.1016/B978-044452228-3/50006-6)
1011 044452228-3/50006-6, 1987.

1012 Petersen, J., Barras, C., Bézos, A., La, C., de Nooijer, L. J., Meysman, F. J. R., Mouret, A., Slomp, C. P.,
1013 and Jorissen, F. J.: Mn/Ca intra- and inter-test variability in the benthic foraminifer *Ammonia tepida*,
1014 *Biogeosciences*, 15, 331–348, <https://doi.org/10.5194/bg-15-331-2018>, 2018.

1015 Piez, K. A.: Amino Acid Composition of Some Calcified Proteins, *Science*, 134, 841–842,
1016 <https://doi.org/10.1126/science.134.3482.841>, 1961.

1017 Pytkowicz, R. M.: Rates of Inorganic Calcium Carbonate Nucleation, *The Journal of Geology*, 73, 196–
1018 199, <https://doi.org/10.1086/627056>, 1965.

1019 Raddatz, J., Rüggeberg, A., Margreth, S., and Dullo, W. C.: Paleoenvironmental reconstruction of
1020 Challenger Mound initiation in the Porcupine Seabight, NE Atlantic, *Marine Geology*, 282, 79–90,
1021 <https://doi.org/10.1016/j.margeo.2010.10.019>, 2011.

1022 Raddatz, J., Liebetrau, V., Rüggeberg, A., Hathorne, E., Krabbenhöft, A., Eisenhauer, A., Böhm, F.,
1023 Vollstaedt, H., Fietzke, J., López Correa, M., Freiwald, A., and Dullo, W. C.: Stable Sr-isotope, Sr/Ca,
1024 Mg/Ca, Li/Ca and Mg/Li ratios in the scleractinian cold-water coral *Lophelia pertusa*, *Chemical*
1025 *Geology*, 352, 143–152, <https://doi.org/10.1016/j.chemgeo.2013.06.013>, 2013.

1026 Raddatz, J., Rüggeberg, A., Flögel, S., Hathorne, E. C., Liebetrau, V., Eisenhauer, A., and Dullo, W. C.:
1027 The influence of seawater pH on U/Ca ratios in the scleractinian cold-water coral *Lophelia pertusa*,
1028 *Biogeosciences*, 11, 1863–1871, <https://doi.org/10.5194/bg-11-1863-2014>, 2014.

1029 Raddatz, J., Nürnberg, D., Tiedemann, R., and Rippert, N.: Southeastern marginal West Pacific Warm
1030 Pool sea-surface and thermocline dynamics during the Pleistocene (2.5–0.5 Ma), *Palaeogeography*,
1031 *Palaeoclimatology*, *Palaeoecology*, 471, 144–156, <https://doi.org/10.1016/j.palaeo.2017.01.024>,
1032 2017.

1033 Raitzsch, M., Duenas-Bohórquez, A., Reichart, G. J., de Nooijer, L. J., and Bickert, T. T.: Incorporation
1034 of Mg and Sr in calcite of cultured benthic foraminifera: Impact of calcium concentration and
1035 associated calcite saturation state, *Biogeosciences*, 7, 869–881, [https://doi.org/10.5194/bg-7-869-](https://doi.org/10.5194/bg-7-869-2010)
1036 2010, 2010.

1037 Raja, R., Saraswati, P. K., Rogers, K., and Iwao, K.: Magnesium and strontium compositions of recent
1038 symbiont-bearing benthic foraminifera, *Marine Micropaleontology*, 58, 31–44,
1039 <https://doi.org/10.1016/j.marmicro.2005.08.001>, 2005.

1040 Rathburn, A. E. and de Deckker, P.: Magnesium and strontium compositions of Recent benthic
1041 foraminifera from the Coral Sea, Australia and Prydz Bay, Antarctica, *Marine Micropaleontology*, 32,
1042 231–248, [https://doi.org/10.1016/S0377-8398\(97\)00028-5](https://doi.org/10.1016/S0377-8398(97)00028-5), 1997.

1043 Schleinkofer, N., Raddatz, J., Freiwald, A., Evans, D., Beuck, L., Rüggeberg, A., and Liebetrau, V.:
1044 Environmental and biological controls on Na/Ca ratios in scleractinian cold-water corals,
1045 *Biogeosciences*, 16, 3565–3582, <https://doi.org/10.5194/bg-16-3565-2019>, 2019.

1046 Schleinkofer, N., Raddatz, J., Evans, D., Gerdes, A., Flögel, S., Voigt, S., Büscher, J. V., and Wisshak, M.:
1047 Compositional variability of Mg/Ca, Sr/Ca, and Na/Ca in the deep-sea bivalve *Acesta excavata*
1048 (Fabricius, 1779), *PLOS ONE*, 16, e0245605, <https://doi.org/10.1371/journal.pone.0245605>, 2021.

1049 Schöne, B. R., Zhang, Z., Jacob, D., Gillikin, D. P., Tütken, T., Garbe-Schönberg, D., McConnaughey, T.,
1050 and Soldati, A.: Effect of organic matrices on the determination of the trace element chemistry (Mg,
1051 Sr, Mg/Ca, Sr/Ca) of aragonitic bivalve shells (*Arctica islandica*) - Comparison of ICP-OES and LA-ICP-
1052 MS data, *Geochemical Journal*, 44, 23–37, <https://doi.org/10.2343/geochemj.1.0045>, 2010.

1053 Schweizer, M., Bowser, S. S., Korsun, S., and Pawlowski, J.: Emendation of *Cibicides antarcticus*
1054 (Saidova, 1975) based on molecular, morphological, and ecological data, *Journal of Foraminiferal*
1055 *Research*, <https://doi.org/10.2113/gsjfr.42.4.340>, 2012.

1056 Secor, C. L., Mills, E. L., Harshbarger, J., Kuntz, H. T., Gutenmann, W. H., and Lisk, D. J.:
1057 Bioaccumulation of toxicants, element and nutrient composition, and soft tissue histology of zebra
1058 mussels (*Dreissena polymorpha*) from New York State waters, *Chemosphere*,
1059 [https://doi.org/10.1016/0045-6535\(93\)90224-S](https://doi.org/10.1016/0045-6535(93)90224-S), 1993.

1060 Segev, E. and Erez, J.: Effect of Mg/Ca ratio in seawater on shell composition in shallow benthic
1061 foraminifera, *Geochemistry, Geophysics, Geosystems*, 7, 1–8,
1062 <https://doi.org/10.1029/2005GC000969>, 2006.

1063 Smith, P. B. and Emiliani, C.: Oxygen-isotope analysis of recent tropical pacific benthonic
1064 foraminifera, *Science*, <https://doi.org/10.1126/science.160.3834.1335>, 1968.

1065 Spero, H. J.: Ultrastructural examination of chamber morphogenesis and biomineralization in the
1066 planktonic foraminifer *Orbulina universa*, *Marine Biology*, 99, 9–20,
1067 <https://doi.org/10.1007/BF00644972>, 1988.

1068 Spötl, C. and Vennemann, T. W.: Continuous-flow isotope ratio mass spectrometric analysis of
1069 carbonate minerals, *Rapid Communications in Mass Spectrometry*, 17, 1004–1006,
1070 <https://doi.org/10.1002/rcm.1010>, 2003.

1071 Stephenson, A. E., Deyoreo, J. J., Wu, L., Wu, K. J., Hoyer, J., and Dove, P. M.: Peptides enhance
1072 magnesium signature in calcite: Insights into origins of vital effects, *Science*, 322, 724–727,
1073 <https://doi.org/10.1126/science.1159417>, 2008.

1074 Sunda, W. G. and Huntsman, S. A.: Regulation of cellular manganese and manganese transport rates
1075 in the unicellular alga *Chlamydomonas*, *Limnology and Oceanography*, 30, 71–80,
1076 <https://doi.org/10.4319/lo.1985.30.1.0071>, 1985.

1077 Swinehart, J. H. and Smith, K. W.: Iron And Manganese Deposition In The Periostraca Of Several
1078 Bivalve Molluscs, *The Biological Bulletin*, 156, 369–381, <https://doi.org/10.2307/1540924>, 1979.

1079 Takesue, R. K., Bacon, C. R., and Thompson, J. K.: Influences of organic matter and calcification rate
1080 on trace elements in aragonitic estuarine bivalve shells, *Geochimica et Cosmochimica Acta*, 72, 5431–
1081 5445, <https://doi.org/10.1016/j.gca.2008.09.003>, 2008.

1082 Tambutté, E., Allemand, D., Zoccola, D., Meibom, A., Lotto, S., Caminiti, N., and Tambutté, S.:
1083 Observations of the tissue-skeleton interface in the scleractinian coral *Stylophora pistillata*, *Coral*
1084 *Reefs*, 26, 517–529, <https://doi.org/10.1007/s00338-007-0263-5>, 2007.

1085 Todd, R.: A new *Rosalina* (foraminifera) parasitic on a bivalve, *Deep-Sea Research and Oceanographic*
1086 *Abstracts*, 12, 831–837, [https://doi.org/10.1016/0011-7471\(65\)90806-5](https://doi.org/10.1016/0011-7471(65)90806-5), 1965.

1087 Toyofuku, T., Kitazato, H., Kawahata, H., Tsuchiya, M., and Nohara, M.: Evaluation of Mg/Ca
1088 thermometry in foraminifera: Comparison of experimental results and measurements in nature,
1089 *Paleoceanography*, 15, 456–464, <https://doi.org/10.1029/1999PA000460>, 2000.

1090 Toyofuku, T., Matsuo, M. Y., de Nooijer, L. J., Nagai, Y., Kawada, S., Fujita, K., Reichart, G. J., Nomaki,
1091 H., Tsuchiya, M., Sakaguchi, H., and Kitazato, H.: Proton pumping accompanies calcification in
1092 foraminifera, *Nature Communications*, 8, 1–6, <https://doi.org/10.1038/ncomms14145>, 2017.

1093 Tribouillard, N., Algeo, T. J., Lyons, T., and Riboulleau, A.: Trace metals as paleoredox and
1094 paleoproductivity proxies: An update, *Chemical Geology*, 232, 12–32,
1095 <https://doi.org/10.1016/j.chemgeo.2006.02.012>, 2006.

1096 Vénec-Peyré, M. T.: Bioeroding foraminifera: A review, *Marine Micropaleontology*, 28, 19–30,
1097 [https://doi.org/10.1016/0377-8398\(95\)00037-2](https://doi.org/10.1016/0377-8398(95)00037-2), 1996.

1098 de Villiers, S., Nelson, B. K., and Chivas, A.: Biological Control on Coral Sr/Ca and $\delta^{18}\text{O}$
1099 Reconstructions of Sea Surface Temperatures, *Science*, 269, 1247–1249, 1995.

1100 Wada, K. and Fujinuki, T.: Biomineralization in bivalve molluscs with emphasis on the chemical
1101 composition of the extrapallial fluid, Book chapter, 1976.

1102 Walker, S. E., Hancock, L. G., and Bowser, S. S.: Diversity, biogeography, body size and fossil record of
1103 parasitic and suspected parasitic foraminifera: A review, *Journal of Foraminiferal Research*, 47, 34–
1104 55, <https://doi.org/10.2113/gsjfr.47.1.34>, 2017.

1105 Webb, A. E., Pomponi, S. A., van Duyl, F. C., Reichart, G. J., and de Nooijer, L. J.: pH Regulation and
1106 Tissue Coordination Pathways Promote Calcium Carbonate Bioerosion by Excavating Sponges,
1107 *Scientific Reports*, 9, 1–10, <https://doi.org/10.1038/s41598-018-36702-8>, 2019.

1108 Whitney, N. M., Johnson, B. J., Dostie, P. T., Luzier, K., and Wanamaker, A. D.: Paired bulk organic and
1109 individual amino acid $\delta^{15}\text{N}$ analyses of bivalve shell periostracum: A paleoceanographic proxy for
1110 water source variability and nitrogen cycling processes, *Geochimica et Cosmochimica Acta*, 254, 67–
1111 85, <https://doi.org/10.1016/j.gca.2019.03.019>, 2019.

1112 Wilbur, K. M. and Saleuddin, A. S. M.: Shell Formation, in: *The Mollusca*, Elsevier, 235–287,
1113 <https://doi.org/10.1016/B978-0-12-751404-8.50014-1>, 1983.

1114 Yin, Y., Huang, J., Paine, M. L., Reinhold, V. N., and Chasteen, N. D.: Structural Characterization of the
1115 Major Extrapallial Fluid Protein of the Mollusc *Mytilus edulis* : Implications for Function,
1116 *Biochemistry*, 44, 10720–10731, <https://doi.org/10.1021/bi0505565>, 2005.

1117 Yu, X. and Inesi, G.: Variable stoichiometric efficiency of Ca^{2+} and Sr^{2+} transport by the sarcoplasmic
1118 reticulum ATPase, *Journal of Biological Chemistry*, 270, 4361–4367,
1119 <https://doi.org/10.1074/jbc.270.9.4361>, 1995.

1120 Zhang, C. and Zhang, R.: Matrix proteins in the outer shells of molluscs, *Marine Biotechnology*, 8,
1121 572–586, <https://doi.org/10.1007/s10126-005-6029-6>, 2006.

1122

1123